Master's Thesis

High molecular weight carboxymethyl cellulose binder to enhance integrity of silicon anodes for Li-ion batteries

Joowon Kang

Department of Energy Engineering

(Battery Science and Technology)

Graduate School of UNIST

2019

High molecular weight carboxymethyl cellulose binder to enhance integrity of silicon anodes for Li-ion batteries

Joowon Kang

Department of Energy Engineering
(Battery Science and Technology)

Graduate School of UNIST

High molecular weight carboxymethyl cellulose binder to enhance integrity of silicon anodes for Li-ion batteries

A thesis
submitted to the Graduate School of UNIST
in partial fulfillment of the
requirements for the degree of
Master of Science

Joowon Kang

12. 05. 2018
Approved by

Advisor
Jaephil Cho

High molecular weight carboxymethyl cellulose binder to enhance integrity of silicon anodes for Li-ion batteries

Joowon Kang

This certifies that the thesis of Joowon Kang is approved.

12. 05. 2018

Advisor: Jaephil Cho

Kyeong-Min Jeong

Nam-Soon Choi

Abstract

Today, considerable interest for eco-friendly and renewable energy systems has been increased toward. Among sustainable energy systems, lithium-ion batteries have been treated as a promising energy device for high-energy batteries. Among anode materials, silicon has attracted attention as a promising candidate for high-energy LIBs due to its high theoretical capacity. However, electrochemical reactions of silicon materials normally result in electrode failure, which cause cell degradation due to massive volume changes upon cycling. To resolve problems, many researchers have studied outstanding binders, which are efficient to sustain the mechanical integrity of electrodes and electrical conductivity, leading to improved electrochemical performances. Herein, we discuss recent works and main issues for functional binders and provide binding mechanisms in terms of chemical and physical features. The relationship between chain lengths of CMC binders and enhanced electrochemical performances of silicon-graphite composite anodes is discussed in detail.

Contents

List of Figures

Figure 26. EDX images of H-MW CMC/SBR composite thin films. The composition of CMC:SBR = 1:1. This thickness is approximately 150 nm.

Figure 27. (a) The image of high-resolution STEM for H-MW CMC/SBR composite thin films. (b) Electron energy loss spectroscopy (EELS) graphs for CMC, SBR, and the interface between CMC and SBR.

List of Tables

I. Introduction

Ever-growing energy needs and limited fossil-fuel resources demand the sustainable energy alternatives, including eco-friendly and renewable energy systems. Among various energy devices, lithium-ion batteries (LIBs) are currently considered as efficient energy devices because of its relatively high gravimetric and volumetric energy density (figure 1). In addition, it has a high productivity which can be manufactured from compact to large sizes for the pursuit of distributed locations.[1] Massive research efforts are underway to develop LIBs because of its little environmental pollution and high energy efficiency.[2, 3] The first commercialized lithium-ion battery was introduced by Sony Corporation in the early 1990s based on the use of lithium intercalation materials. Graphite is representative anode materials, having layered structures of graphene layers and its theoretical capacity is 372 mAh g^{-1}.[4] However, there are limitations for usage of graphite for large scale high-capacity batteries such as EVs and ESS because graphite has relatively low theoretical capacities.[2, 4, 5] Figure 2a and 2b show volumetric and gravimetric discharge capacities for various type of anode materials. The next challenging anode materials are alloying types such as silicon and Tin. Among these anode materials, silicon has quite high theoretical capacity (~4200 mAh g^{-1}), and the working potentials are suitable (table 1).[6-10] The electrochemical reaction of silicon with lithium is alloying reactions that 4.4 lithium atoms could be alloyed to one silicon atom therefore, theoretical capacity of silicon is 10 times higher than that of graphite.[10]

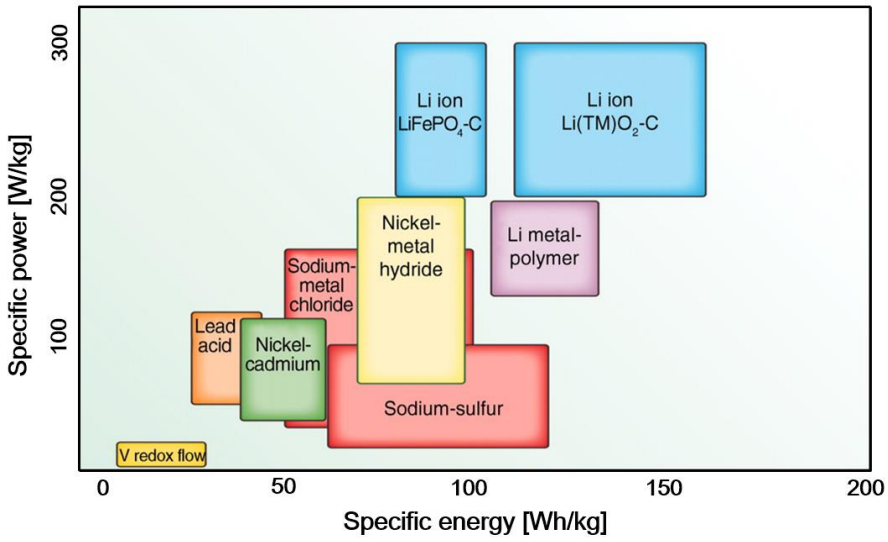

Figure 1. Gravimetric energy density and power density for various kinds of rechargeable batteries.[3]

Materials	Li	C	$Li_4Ti_5O_{12}$	**Si**	Sn	Sb	Al
Density (g cm^{-3})	0.53	2.25	3.5	2.3	7.3	6.7	2.7
Lithiated phase	Li	LiC_6	$Li_7Ti_5O_{12}$	$Li_{4.4}Si$	$Li_{4.4}Sn$	Li_3Sb	LiAl
Theoretical specific capacity (mAh g^{-1})	3862	372	175	4200	994	660	993
Volume change (%)	100	12	1	420	260	200	96
Potential versus Li (V)	0	0.05	1.6	0.4	0.6	0.9	0.3

Table 1. Comparisons of various anode active materials.[7]

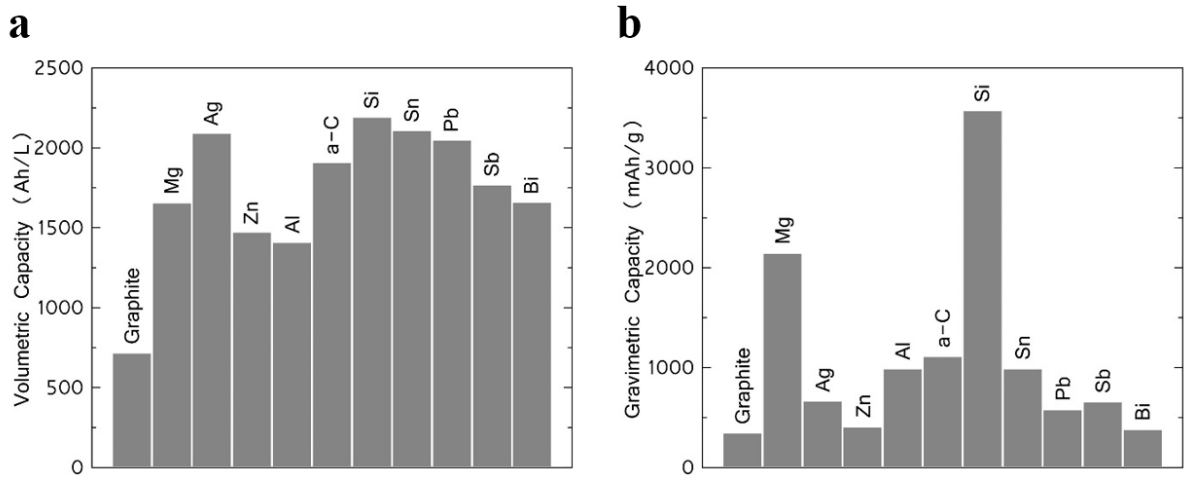

Figure 2. (a) Volumetric capacities and (b) gravimetric capacities of anode material elements.[10]

1.1 Problems of silicon materials

Although silicon materials have high theoretical capacity, their performances are limited by severe volume expansions during charge and discharge. Their high volumetric expansion on lithiation leads to limited cycle ability and low rate capability.[7, 10] Figure 3 shows degradation processes of electrodes with silicon nanoparticles (SNPs). First drawback is the cracking within a silicon particle which induces isolated particles as shown in figure 3a. During charging and discharging, silicon particles could not withstand massive mechanical stress. Therefore, the capacity is drastically decreased by losing electrical contacts. Significant research effort has been devoted to mitigate expansions of silicon materials in recent years.[7-10] Figure 4 shows various strategies for silicon materials to prevent massive volume expansion. Kim et al. suggested that silicon nanocrystals with homogeneous distribution of carbon coating improve rate capability, which alleviate severe volume expansions of silicon materials. In addition, they showed that cycle performances and initial coulombic efficiency (I.C.E.) were improved.[11]

Secondly, huge volume change of silicon particles leads to continuous growth of solid electrolyte interphase (SEI) layers leading to drastic capacity fading during the lithiation and de-lithiation (figure 3b). Liu's group reported that void space engineering that single silicon nanoparticles are encapsulated by carbon layers leaves enough void space for expansion and contraction during charge and discharge. It prevents the excess growth of SEI layers and increases integrity of materials, leading improved cycle properties (figure 4).[12]

The third one is the fracture of the electrodes, which results in loss of electrical and mechanical integrity of electrodes with pulverization and fractures during cycling (figure 3c). This leads to exfoliation of the electrode composites from the current collectors. Recently, much attention has been increased to developing functional binders that could improve integrity of the electrodes with silicon particles.[13-20]

As shown in figure 5a, Bonjae et al. reported that condensation reactions between carboxylic acid groups of polyacrylic acid (PAA) and hydroxy moieties of carboxy methyl cellulose (CMC) could form inter-chain cross linking binders, exhibiting enhanced mechanical strength of electrodes and improved cycle performances with silicon nanoparticles (SNPs) by analyzing fourier transform-infrared (FT-IR) and X-ray photoelectron spectroscopy (XPS).[16, 21, 22]

Fig 5b shows that the report of Jiangxuan's group that polymer networking from esterification reactions between polyacrylic acid (PAA) and polyvinyl alcohol (PVA) improves cycleability and initial coulombic efficiency (I.C.E.) of electrodes with SNPs. As shown figure 5b, the cell with PVDF binder shows a drastically decreased capacity after 50 cycles. In contrast, the cell with PAA/PVA binder exhibits better cycling stability (2283 mAh g^{-1} after 100 cycles).[19, 22] Such attractive properties of binders have enable to silicon materials as anode electrodes in high capacity batteries, resulting in

improved cycle ability.

As shown in figure 5c, Mingyan et al. improved cycle performances by synthesizing conductive binders which act as conducting agents and binder. PEFM binders have four kinds of polymer chain. Polyfluorene with octyl side chains (P) plays a role in increasing electronic conductivity and mechanical strength by adding long octane chains. Fluorene with triethyleneoxide monomethyl ether side chains (E) can increase uptake of electrolyte. Fluorenone (F) has enriched electrons in fluorine therefore, it could optimize electronic conductivity. Methyl benzoate ester (M) improves flexibility of chain and mechanical adhesion. Therefore, the PEFM binder could maintain the electrical conductivity and mechanical integrity upon cycling.[18, 22]

Chao's group suggested that self-healing binders could recombine fractured structures with spontaneous hydrogen bonding, leading improved cycleability and rate performances. They ascribed that the properties of amorphous polymer with low value of T_g enable to generate driving force to make hydrogen bonds, resulting in the dynamic re-association. It alleviates degradation of the electrodes with silicon materials and improve cycle performances during charge and discharge process (figure 5d).[17, 22]

These researches suggest that the strong interaction between these functional groups of binder and surface of silicon active materials are favorable for improving mechanical strength and electrochemical performances.[19]

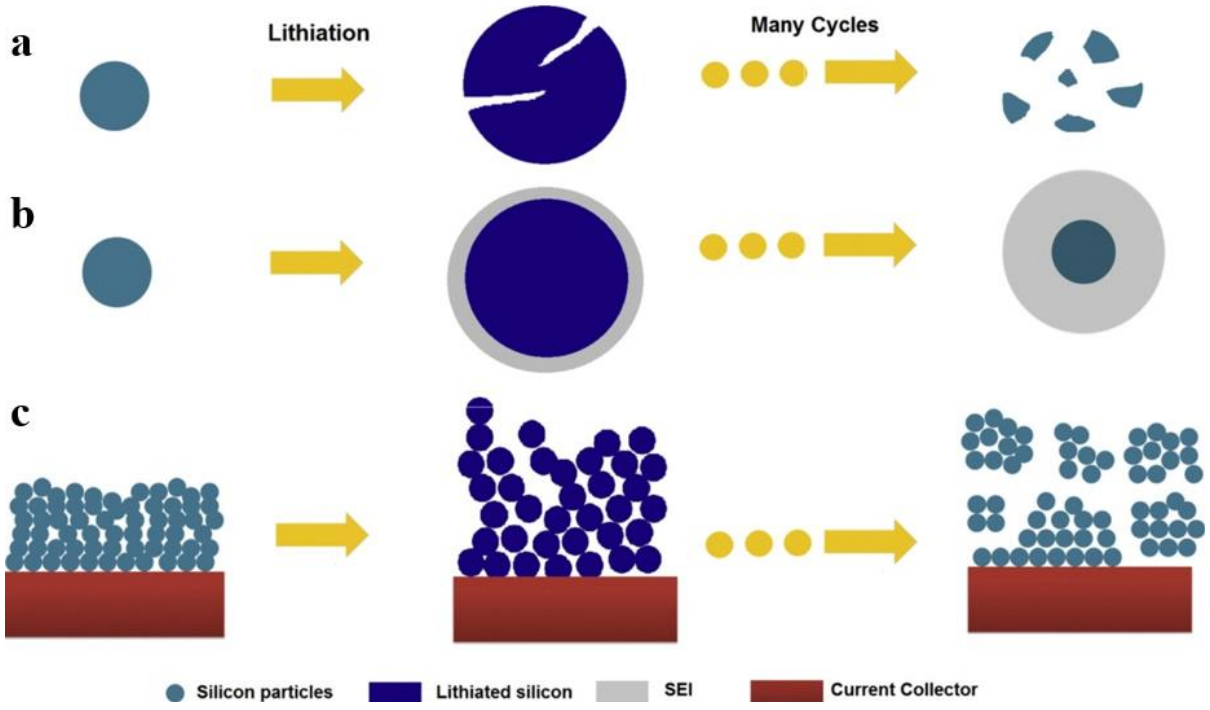

Figure 3. Degradation processes of electrodes with silicon nanoparticles (SNPs) (a) Particle pulverization upon expansion and contraction of SNPs. (b) Continuous SEI layer growth at the interface between silicon particles and electrolytes during lithiation and delithiation. (c) Electrode failure of silicon negative electrode upon cycling.[7]

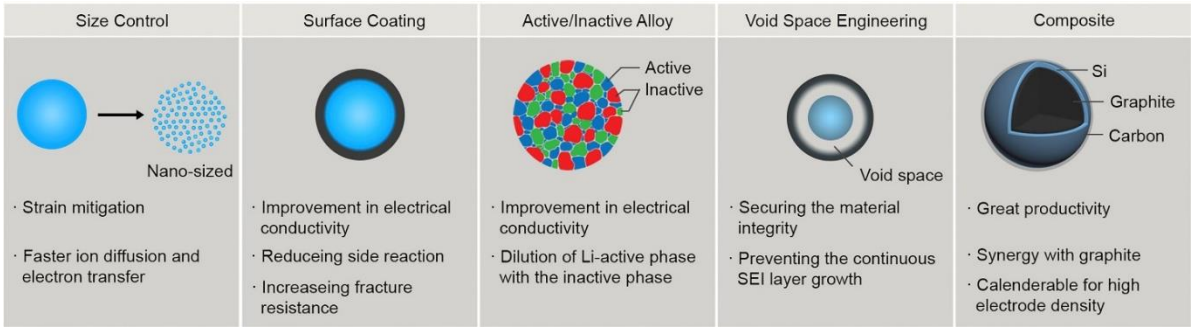

Figure 4. Various strategies for silicon materials to prevent massive volume expansion.[9]

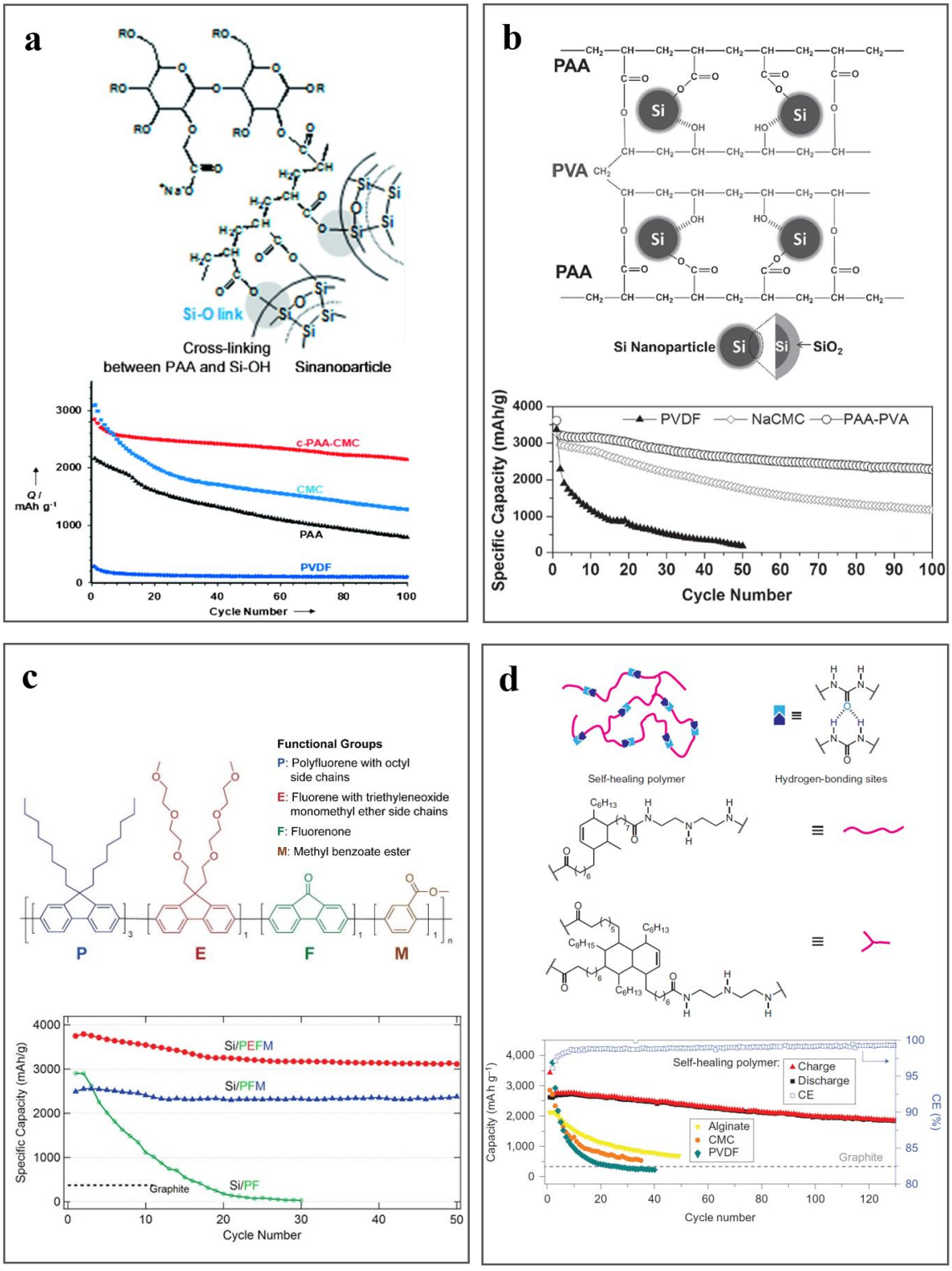

Figure 5. Recent researches in functional binders to enhance cycle performance for silicon anode materials. (a) PAA-CMC cross-linked binders.[16] (b) PAA/PVA binders.[19] (c) PEFM conductive binders.[18] (d) Self-healing binders.[17]

1.2 Various kinds of representative commercial binders

Binders are used to link active materials and conducting agents to retain these composites bonded on the current collectors. Figure 6 shows the structures of various anode binders, for example, polyacrylic acid (PAA), polyvinyl alcohol (PVA), polyvynylidene fluoride (PVDF), styrene butadiene rubber (SBR), and carboxymethyl cellulose (CMC). In recent research, an outstanding binder is effective to sustain the mechanical properties of electrodes, leading to improved electrochemical performances of cells. In particular, enhanced adhesion properties could mitigate particle pulverization of alloying materials such as silicon and Tin, resulting in better life time. In addition, it contributes to increase viscosity for electrode fabrications and acts as the surface modifications.[13, 23, 24] Prerequisites of efficient binders are 1) cheap prices, 2) electrochemical stability, 3) sufficient binding forces with particles, and 4) high adhesion to current collectors to retain integrity of electrodes after subsequent cycling.[24-30]

1.2.1 Polyvynylidene fluoride (PVDF)

PVDF is a commercialized binder for both positive and negative electrodes owing to the good electrochemical stability and strong adhesion forces. However, organic solvents such as NMP are required for a slurry production due to its water-insoluble natures. The inherent limitations of organic solvents, such as expensive price, flammable, volatile, and occurrences of environmental pollution hinder their practical use.[25, 27, 31] As shown in figure 6c, PVDF polymer is dispersed by the steric stabilization dispersion mechanism due to having only fluorine groups, resulting relatively high elasticity.[28, 31, 32] This flexible nature of PVDF wraps around the surface of active materials and acts as a surface modifier affecting physical and electrochemical properties. Especially it acts as a passivation layer in active materials with lithium cobalt oxide, nickel cobalt manganese oxide and lithium titanium oxide. Therefore, it can reduce an irreversible capacity and increase an initial coulombic effeciency.[23, 30] Therefore, PVDF binder works well for LCO, Ni-rich cathode materials and carbonaceous materials that have only a 10% volume expansion. [23-25, 30, 33] However, due to the low fracture stresses and rupture strengths, PVDF binder cannot afford sufficient bonding with alloying type of anode materials that exhibit massive volume expansions upon cycling. Figure 7a shows stress vs. strain for PVDF, CMC, and CMC+SBR binder films. PVDF films has a relatively low offset yield point which is a point on intersection between original graph and the graph with proportional limit slope at 0.2% strain. Considering that the volume change of silicon materials is up to 300%, the PVDF binder could not accommodate electrode expansions upon cycling. As shown in figure 7b, the silicon anodes with PVDF binders show fast capacity fading and deterioration of the electrode during charge and discharge process.[25, 30-32] Figure 7c is simple schematic illustrations of PVDF and CMC binders for silicon anode materials during discharge and charge, which shows that the PVDF films could not sustain its elasiticity.[14].

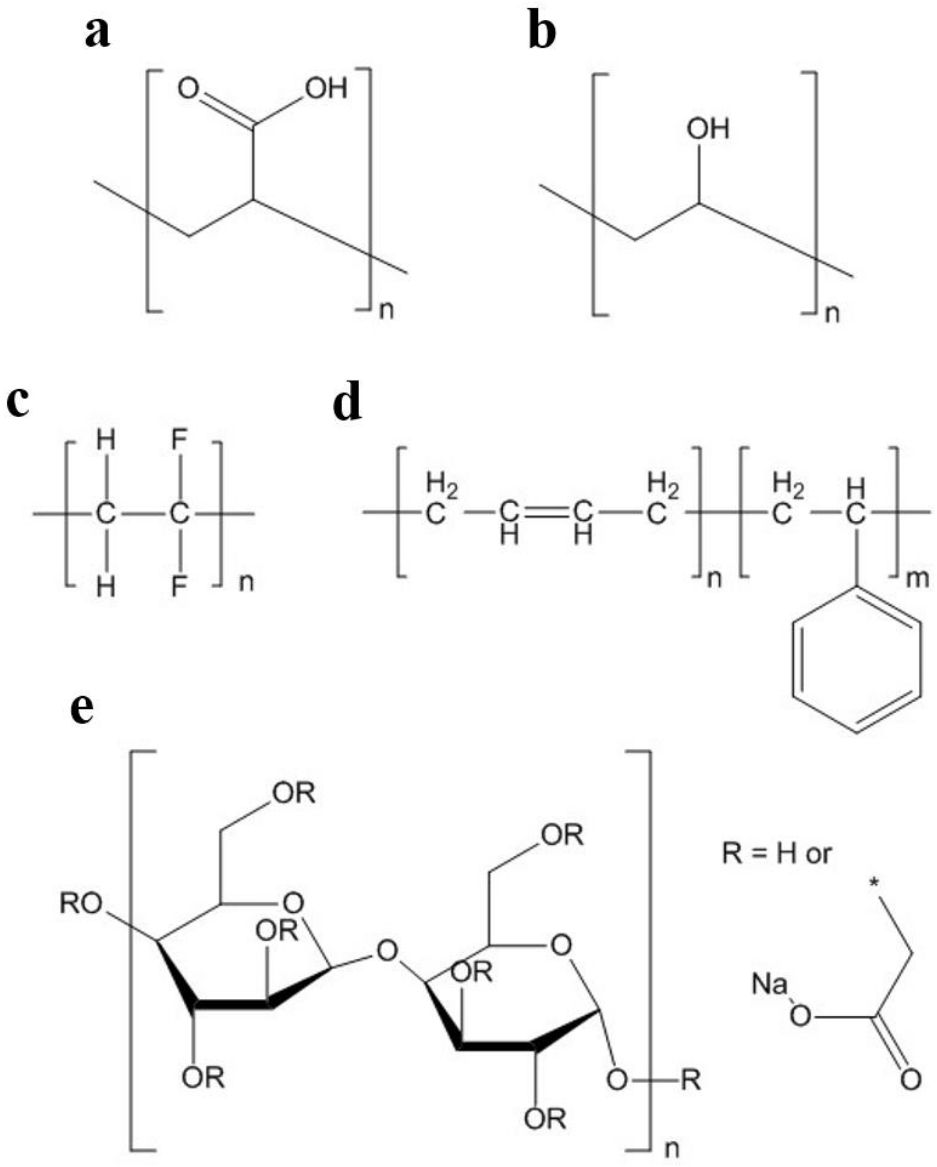

Figure 6. The structures of (a) Polyacrylic acid (PAA), (b) Polyvinyl alcohol (PVA), (c) Polyvynylidene fluoride (PVDF), (d) Styrene butadiene rubber (SBR), and (e) Carboxymethyl cellulose (CMC).

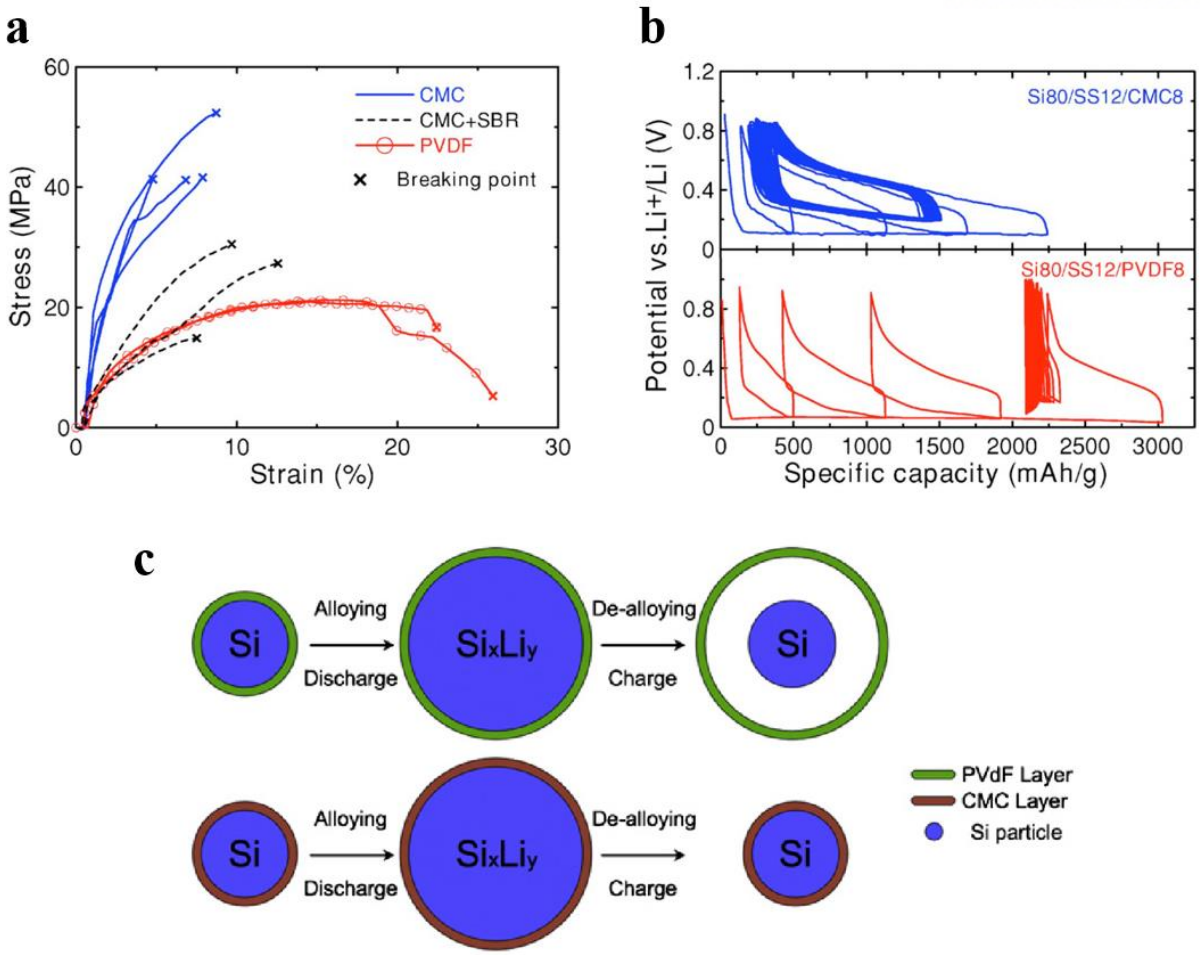

Figure 7. (a) Stress vs. strain curves for CMC, CMC-SBR composite, and PVDF films. The x points represent fracture stress point (or rupture stress point) at the end of each curve. (b) Potential vs. specific capacity curves during four formation and 70 cycles of silicon negative electrodes. The electrodes were discharged to 500, 1000, 1500 and 2000 mAh g^{-1} and charged to 0.9 V, respectively then were cycled with current density of 150 mA g^{-1} between 0.17 V and 0.9 V. The notations of Si80/SS12/CMC8 and Si80/SS12/PVDF8 represent the electrode was consisted with 80 wt.% of Si powder, 12 wt.% of Super-S carbon black and 8 wt.% of CMC and PVDF, respectively.[30] (c) The simple schematic illustrations of PVDF and CMC binders for silicon anode materials during discharge and charge.[14]

1.2.2 Carboxymethyl cellulose (CMC)

Carboxymethyl cellulose is one of the polysaccharide polymers having high-modulus natural. Compared with non-functional binders such as PVDF and SBR, CMC has various functional groups such as hydroxyl, carboxyl acids, and carboxylates. As shown in figure 7a, CMC films retain elastic deformation until the stress of 40 Mpa owing to its rigid and hard structures of cellulose ring backbones.[22, 24] As shown in figure 7b, cycle retention of the electrode with CMC binder were better than PVDF electrodes. This is because high-modulus nature properties and various polar functional groups of CMC binder could retain integrity of electrodes with SNPs. In addition, CMC binder plays an additional role as a surface modifier which reduces surface resistances by forming passivation layers.[30] These properties was determined by 1) values of degree of substitution, 2) lengths of a polymeric chain, and 3) types of counter ions.[23-25, 33]

1) Degree of Substitution (DS)

Degree of substitution (DS) describes an average value, indicating the extent of substitution which hydroxyl group of CMC has been replaced by a carboxymethyl group per one unit length. The maximum value of DS is 3, because there are three OH groups per a cellulose ring (C_6). The higher value of DS, the higher number of substituted to carboxymethyl groups. Figure 8a shows adsorption isotherms for CMC on natural graphite. It shows that less substituted CMC binder (DS 0.7) was more adsorbed on the surface of natural graphite than more substituted CMC binder (DS 1.28). This is because substituted methyl groups have anionic charge in the solvent and interact with solvent molecule favorably, resulting in reduced interaction with active materials. This results in reduced bonding points on the surface of active materials because the interaction of the hydrophilic carboxylate groups with an aqueous solvent is greater than that with the surface of active materials.[24, 26, 34] Figure 8b shows cycle curves for each DS values of CMC on natural graphite. The CMC binder with DS 0.7 has better cycle performances than that with DS 1.28. The adsorbed CMC binders on the surface of active materials play a role of passivation layer which reduce side reactions with electrolytes, leading improved long cycle life. The carboxyl acid groups of CMC binder form covalent bonds with hydroxyl groups on the surface of active materials.

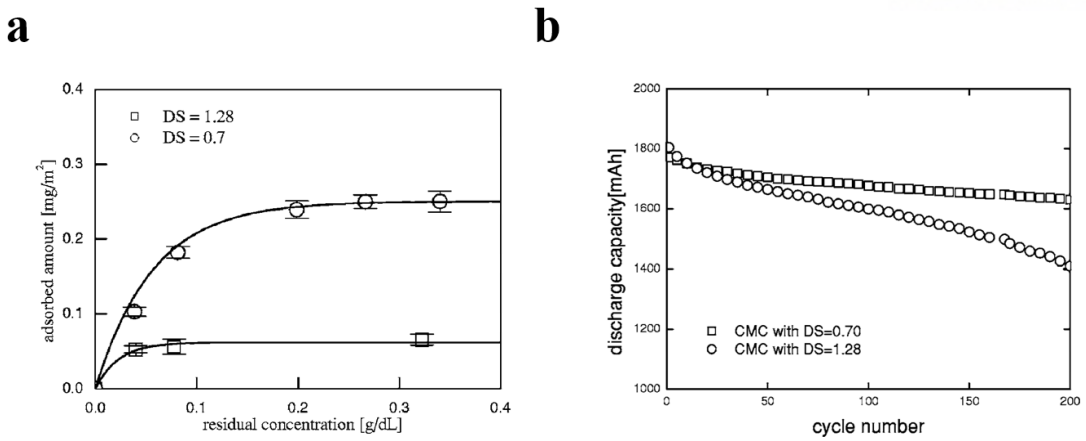

Figure 8. (a) Adsorption isotherms for CMC on natural graphite.[24, 34] (b) Cycle curves for each DS values of CMC on natural graphite.[24]

2) Chain lengths

The chain lengths influence on inter-molecular interactions among binder molecules. The chain of CMC binders which has linear and rigid structures becomes extended conformation in the solvent by elevating molecular weights. In this feature, the higher molecular weight, the larger dynamic hydration radius of dispersed CMC polymers in the solvent. The size of extended chain lengths affect the electrochemical properties of silicon anodes. Figure 9a is a voltage profile and cycle graphs of CMC binders having different molecular weight, CMC 250,000 g mol^{-1} and CMC 700,000 g mol^{-1} respectively. As seen from figure 9a, charge and discharge capacity of CMC 700,000 were higher than that of CMC 250,000, as well as coulombic efficiency. Bridel et al. explained that the inter-molecular force of binders influences on both electrochemical and mechanical properties of electrodes with silicon materials. They analyzed inter-molecular forces among binder molecules by measuring intrinsic viscosity and showed that the intrinsic viscosity of CMC 700,000 was higher than that of CMC 250,000. Figure 9b and 9c show the intrinsic viscosity (L mol^{-1}) and capacity (mAh g^{-1}) of silicon anodes corresponding to degree of substitution with CMC 250,000 g mol^{-1} and CMC 700,000 g mol^{-1} respectively. As seen from figure 9b and 9c, the intrinsic viscosity of CMC 700,000 was higher than that of CMC 250,000 at the same DS value. It was considered that inter-molecular interactions of higher molecular weight binder could be more saturated than that of lower molecular weight binder. In addition, it showed that the charge and discharge capacity were proportional to the intrinsic viscosity. Inter-molecular forces among high molecular weight polymers are stronger than that of low molecular weight polymers because massive molecules have strong van der Waals interactions.[26, 31, 33, 34] As a result, high molecular weight binder is more adsorbed at the surface of active materials, reducing side

reaction and forming stable SEI layers. Thus, it improves the lifetime of cells. [24, 33, 35]

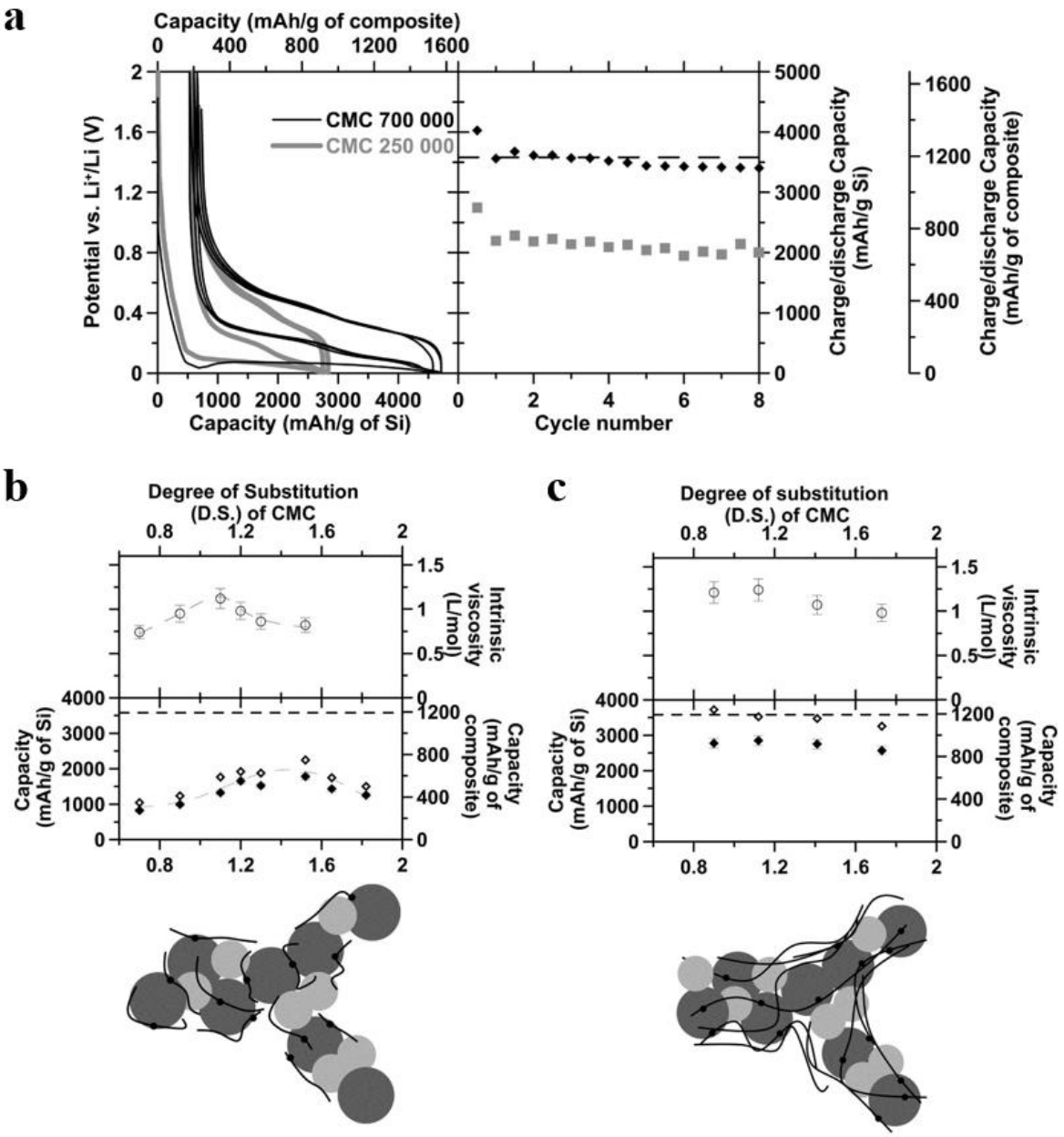

Figure 9. (a) Potential vs. specific capacity curves and cycle graphs with two kinds of CMC binders having different molecular weight, CMC 250,000 g mol^{-1} and 700,000 g mol^{-1} respectively. (b) The intrinsic viscosity (L mol^{-1}) and capacity (mAh g^{-1}) of silicon anodes with CMC 250,000 g mol^{-1} corresponding to degree of substitution. (c) The intrinsic viscosity (L mol^{-1}) and capacity (mAh g^{-1}) of silicon anodes with CMC 700,000 g mol^{-1} corresponding to degree of substitution.[33]

3) Types of counter ions

Depending on the types counter cations, an ability of dissociation was determined by size of radius. Generally, small sized cations are difficult to dissociate because a small sized cation has strong ionic interactions between cations and anions. For this reason, smaller size cations are difficult to dissociate in aqueous solvents than that of large size cations. It influences to disperse polymer in solvents by forming various size of conformation. The smaller the monovalent cation is, the lower its dissociation in solution and will be buckling of the chains.[26, 33]

In general, CMC binder acts as a thickening agent which could maintain proper viscosity for negative electrode suspensions and surface modifiers which reduces side reactions resulting in stable SEI layers on the surface of active materials.[23, 26, 30, 31, 34] Polar-functional groups improve the physical stability of electrodes and electrochemical properties than that of non-functional binders such as PVDF and SBR.[29]

1.3 Binding mechanisms

Binder plays a role of binding between particles and adhering electrode composite onto the current collectors. The binding activity was affected nature properties of polymeric bonders such as constituent element, chain length, and crystallinities. These factors determine the conformation which represent the size and shape of dispersed polymer in the solvents. In addition, various functional groups of polymer could form chemical bonds such as hydrogen bonds and covalent bonds with active materials and current collectors, leading enhanced adhesion forces of electrodes. Especially, CMC has more complex conformations than other polymer binders because it has a variety of functional groups,.[26, 28] The conformation plays an important role in determining physical properties of electrodes such as the viscosity, stability of slurries, a porosity of electrode, and textures of the electrode. Figure 10a is the atomic force microscope (AFM) image of dried CMC binders onto the highly ordered pyrolytic graphite (HOPG). The HOPG was immersed in the CMC solution with concentration of 0.2 wt.% during several hours then dried at 60°C. From figure 10a, it was confirmed that CMC binder tends to form network structures.[23] Figure 10b is the SEM image of peeled pristine electrode with silicon-graphite composite, super-P carbon black, CMC binder, and SBR. It shows that CMC binder is adsorbed on the active material surface and forms binder networks with conducting agents. Figure 10c and 10d are the SEM images of peeled pristine electrodes, which show network structures between current collectors and active materials, leading improved adhesion.

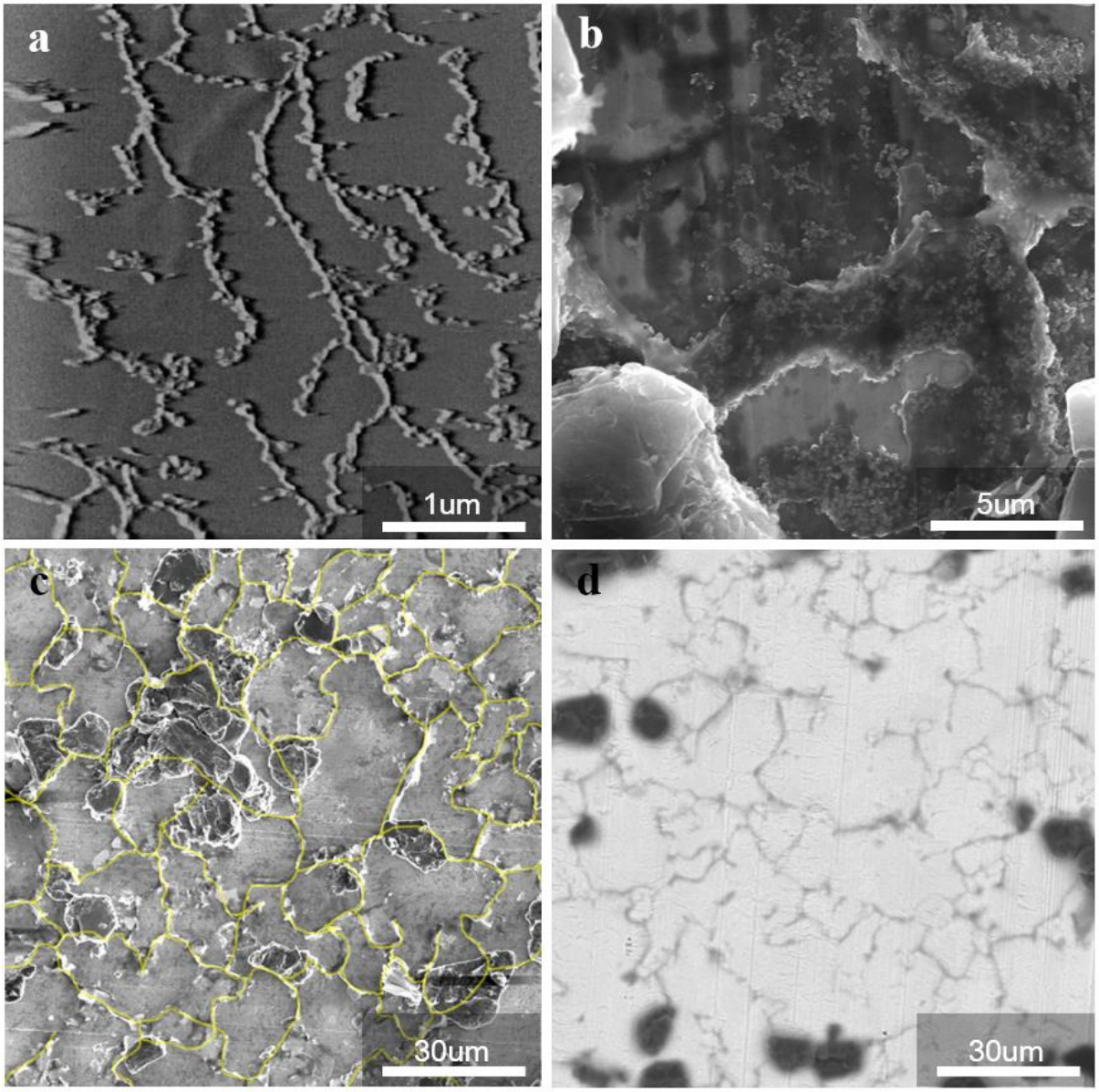

Figure 10. (a) AFM images of CMC binder film on the highly ordered pyrolytic graphite (HOPG).[23] (b), (c), (d) SEM images of copper foil side of silicon-graphite composite electrode peeled by INSTRON equipment.

1.3.1 The dispersed conformations

Conformation is the macroscopic shape and size of dispersed polymer chains in the solvent. Many different types of conformations are affected by molecular weight, functional groups, salts, and nature of polymer backbones. It not only influences viscosity during slurry manufacturing but also affects integrity of electrodes, forming three dimensional networks. In general, large size of conformation has strong inter-molecular force and high viscosity, leading enhanced adhesion strength. This suggests that adhesion strength vary depending on dispersed size of conformation and morphology of adsorbed polymer on the surface of active materials. After solvent evaporation, dried composites of electrode try to retain the slurry conditioning morphology and are tighten altogether.[13, 29, 36]

1) **Intra-molecular interaction** is the attractive and repulsive interaction that occurs within a molecule. There are several factors which influence to shape and size of conformations, such as ionic force, chain length, and hydrogen bonds. Ionic repulsive force is the main factor that induced by dissolution of functional groups such as hydroxyl (-OH), carboxyl (-COOH) and cyanide (-CN). The larger the functional size, the more anionic repulsive interaction. In addition, chain lengths affect to size of conformation. This could be due to that the rigid backbones cause the extended conformations thereby increasing hydrodynamic volume. Also, hydrogen bonds affects to attractive interactions among various functional groups.[13, 14]

2) **Inter-molecular interaction** is the macroscopic interactions among two or more polymer molecules. Desirable factors, such as mechanical integration and electrode manufacturing are determined by molecular interactions, resulting improved electrochemical properties. The surface free energy, resulting from degrees of exposed functional groups with the solvent, influences repulsive interactions among molecules. In general, large size conformation has relatively low surface free energy because exposed functional groups with the solvent per area unit are little, resulting in reduced repulsive interaction forces. In addition, all disperse system have van der Waals forces, which called ‘London dispersion forces’, because electrons in molecules undergo fluctuations in time. There are huge electric fields on large size polymer and these fields contribute to formation of dipole moments, resulting in inter-molecular attractive forces.[13, 14, 24, 33]

1.3.2 Chemical bonds

When heat is applied to the coated slurry, dispersed binder conformation is condensed and the composite structure of the electrode is formed. The polar functional groups of the binder contribute to maintain the composite structures of the electrode via hydrogen bonding and covalent bonding.[21, 24, 29-31, 35] Figure 11a shows that the mechanisms for formation of covalent bonds via esterification reaction. As shown in figure 11a, hydroxyl group of silicon anode materials and carboxylic acid group of CMC binder forms covalent bonds through a condensation reaction at temperatures above 150°C.[21, 35] It was confirmed by fourier transform infrared (FT-IR) spectroscopy that the covalent bonding is formed between OH- groups of SiO_2 and COOH- groups of CMC binder at the wavenumber of 1630 cm^{-1} as shown in figure 11b which is the FT-IR data with a silicon material and CMC binders at different pH conditions.[25, 27, 31, 32, 35] Figure 11c is the cycle curves of PVDF, PVA, and PAA with silicon anode materials. As shown in figure 11c, the electrochemical performances of polyacrylic acid (PAA) binder and polyvinyl alcohol (PVA) binder are better than that of PVDF binders. It is because polyacrylic acid (PAA) binder has a carboxyl group which could form a covalent bond through esterification reaction with hydrolysis OH- group of the SiO_2 layers and polyvinyl alcohol (PVA) binder, which has hydroxyl groups, forms strong hydrogen bonds with the functional groups of active materials and current collectors, resulting in enhanced mechanical integrity of.[15] Chemical bonds, such as hydrogen bonds and covalent bonds, are important factors that influence to not only the mechanical properties, but also electrochemical performances such as the SEI layer formation and cycle performances.[13, 28, 37-39]

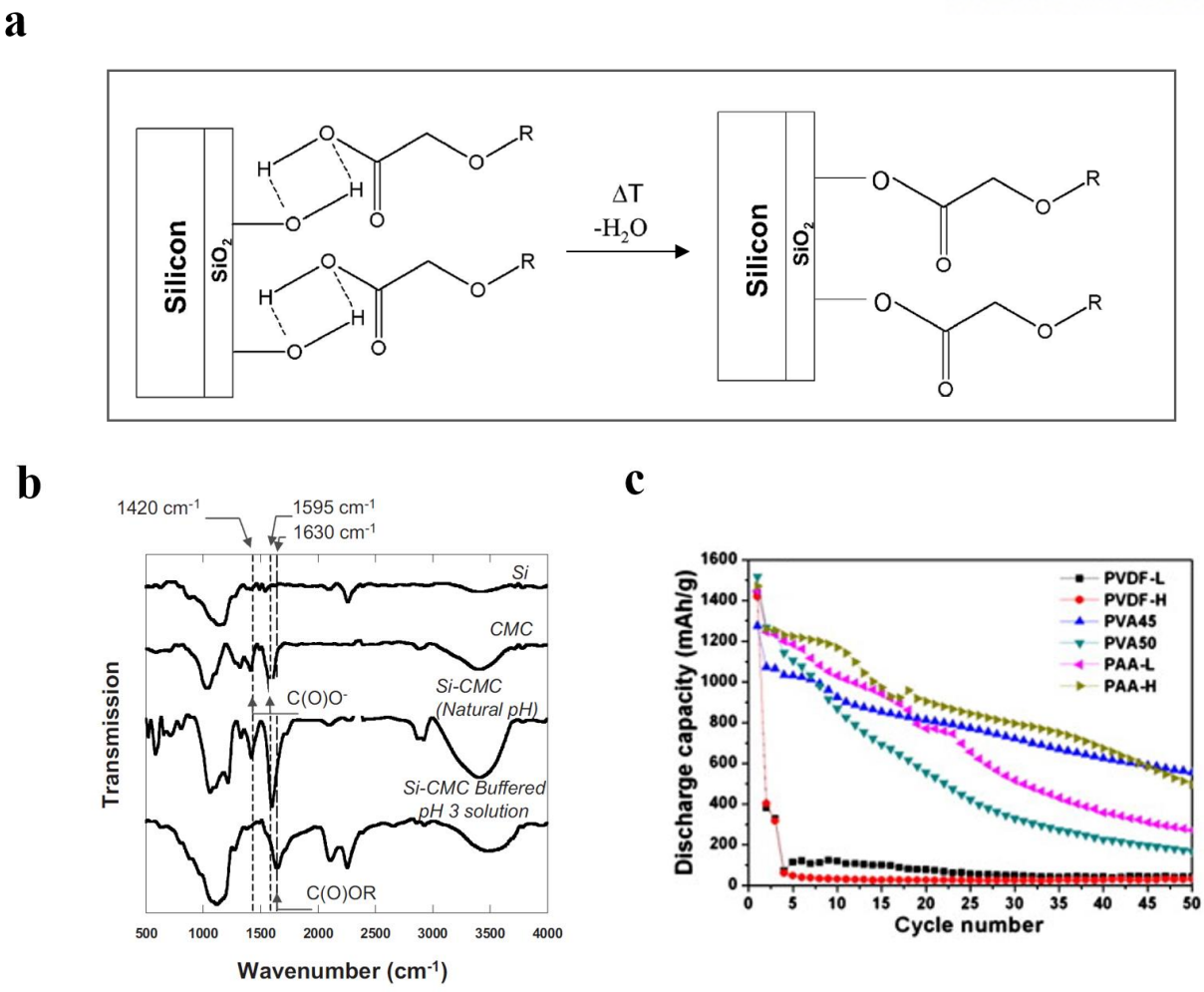

Figure 11. (a) The mechanisms of covalent bond formation via esterification reaction.[21, 36, 40] (b) FT-IR data with silicon material and CMC binder at different pH conditions.[35] (c) The cycle curves of PVDF, PVA, and PAA with silicon anode materials.[15]

1.4 Surface film resistances (Solid Electrolyte Interphases)

Solid electrolyte interphase (SEI) layer plays an important role in determining electrochemical properties of cells such as cycle life, rate capability, and coulombic efficiency. It is formed by oxidation and reduction reactions on the active material, resulting in decomposition of electrolytes and salts. Figure 12a is a potential energy diagram for lithium-ion batteries. This reductive decomposition occurred by reduction of electrolytes, because electrons in lithiated anode active materials with high HOMO energy levels migrate to LUMO energy levels of electrolytes, resulting in SEI films on the surface of active materials. Figure 12b shows schematic illustration of SEI layer, TEM images of surface of graphite, and EDX mapping. All reductive compound such as Li_2CO_3, LiF, and Li_2O are insoluble materials which were formed at first few cycles generally. [41, 42] The stable SEI layer is attributed to thin and compact morphologies, which play an important role for the long cycle life and coulombic efficiency. For these features, additives such as FEC and VC has been used to form compact and dense SEI layers. In addition, functional binders could play as a surface modifiers, resulting in stable SEI layers. Shu' group and Jing' group reported that CMC binder can better bond on the surface of Si particles to form of the stable SEI layer.[22, 30]

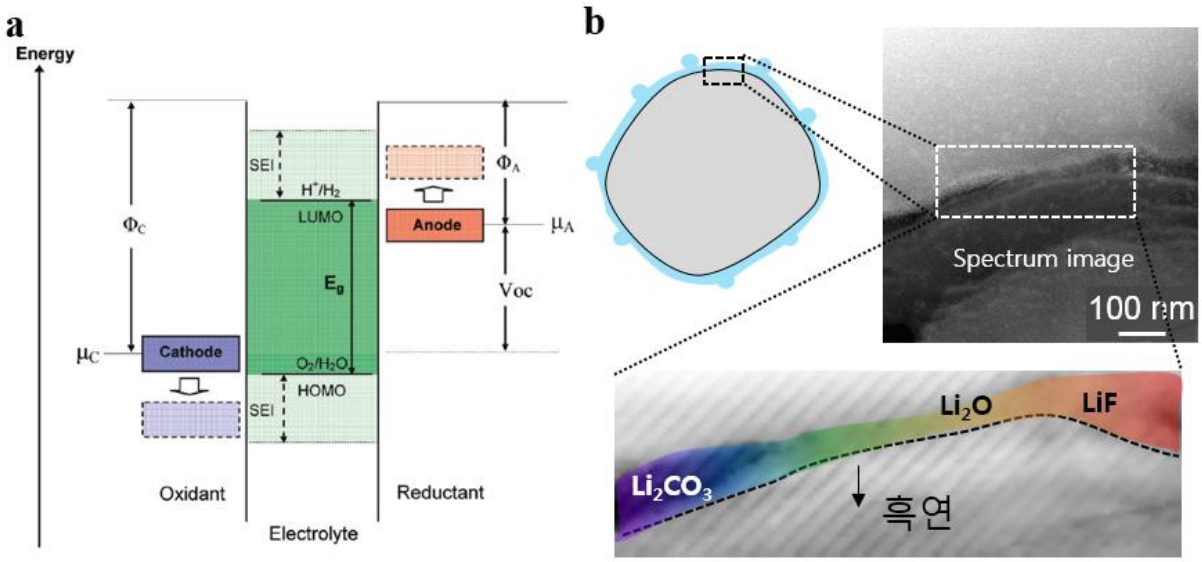

Figure 12. (a) Potential energy diagram for lithium-ion batteries.[43] (b) Schematic illustration of SEI layer, TEM images of surface of graphite, and EDX mapping.

The surface film resistance can be divided into binder resistances and electrolyte decomposition resistances. Zhang et al. showed that the surface resistance was changed enormously at around 0.15 V that the lithiation reactions take place. Figure 13a shows electrochemical impedance spectroscopy (EIS) data of coin half cells. It is observed intrinsic resistances of polymeric binders and decomposition of electrolytes and salts above 0.15V because it is before lithiation, which show little volume expansion. However, after lithiation, the volume expansion of high capacity electrode causes fracture, cracking and pulverization, leading to new formed SEI resistances. It was proved by dQ/dV curves as shown in figure 13b which represents dQ/dV data for Li/graphite half-cell and SEI resistance corresponding potentials.[37, 41, 43] Therefore, increased resistances after lithiation attribute to continuous growth SEI layers due to pulverization and cracks of particles resulting from volume expansion.[37, 41]

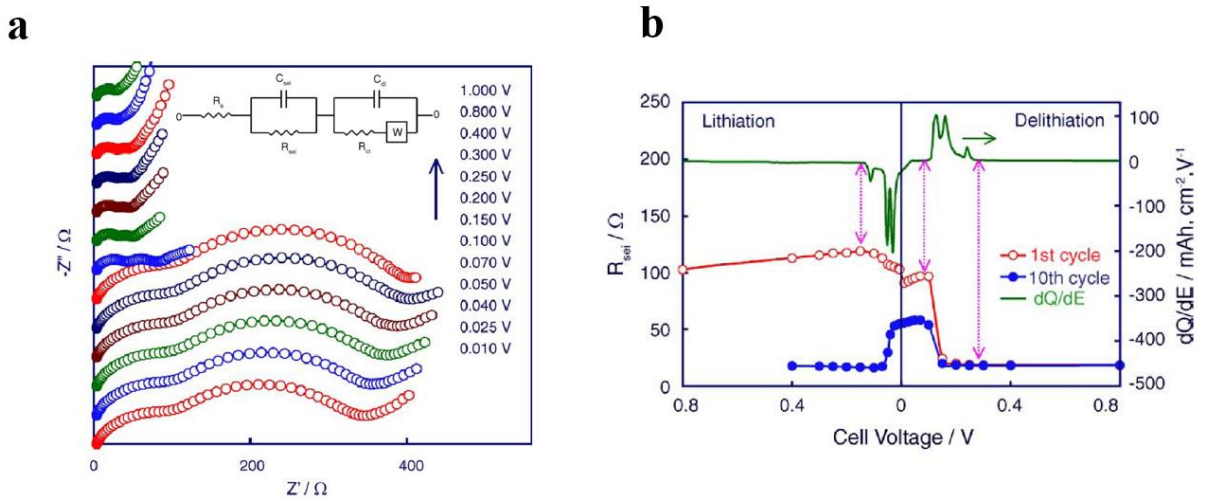

Figure 13. (a) EIS data of the Li/graphite half-cell at various potentials which were conducted during the first de-lithiation process of a cell using 1M $LiPF_6$ and EC/EMC (3:7 wt.%) electrolyte. (b) dQ/dV curves for Li/graphite half-cell and SEI resistance corresponding potentials.[37]

II. Experiments

2.1 Physical property analysis

2.1.1 Hydrodynamic radius

Each CMC-Na powders (L-MW CMC, H-MW CMC, SIGMA-ALDRICH Inc. and M-MW CMC, NIPPON PAPER INDUSTRIES) are dispersed in distilled water with concentration of 0.01 wt.% using homogenizer (3000 rpm, 20 min). Then they are sonicated during 10 min and left for conditioning during 1 hr. These solutions are tested by using a zeta-sizer Nano ZS instrument (Marvern Panalytical, 0.3 nm ~ 10 um) to measure hydrodynamic radius (DLS, dynamic light scattering) and repulsive interactions (zeta-potentials).

2.1.2 Adsorption measurement

SG17 (BTR New Energy Materials Inc.) is used active materials (surface area: 5 cm^2 g^{-1}) and each different CMC solutions was added to the SG17 powder. They then are mixed using homogenizer (3,000 rpm, 1 hr) and left for conditioning overnight. The suspensions were then centrifuged (5,000 rpm, 20 min) and the supernatants pipetted out for evaluation of CMC concentration by Total Organic Carbon instruments (TOC-V, Shimadzu).

$$M_{ads} = (C_{init} - C_{fin})V/m_tA$$

M_{ads} (mg m^{-2}) is the amount of adsorbed CMC on graphite. C_{int} (mg l^{-1}) is the initial CMC concentration. C_{fin} (mg l^{-1}) is the final CMC concentration. V (l) is the total system volume. m_t (g) is the mass of graphite in system. A (m^2 g^{-1}) is the specific surface area of graphite.[34]

2.1.3 Rheology test

Graphite (SG17) and CMC powder are mixed at first step. Second step is making slurry by adding deionized water. Last step is adding emulsion of SBR (Zeon co.) particles (40 wt.%) to the slurry. Homogenizer (5000 rpm each step, 20 min for 1^{st}, 40 min for 2^{nd}, 15 min for last step) is used to disperse all materials for regular particle distributions. Then slurries are left for conditioning overnight. These slurries are measured shear forces associated with a flowing substance between two plate by rheometer (Haake MARS Ⅲ - ORM Package). Viscoelasticity is dynamic mechanical analysis where oscillatory fluctuations are applied to microstructures. From frequency sweep modes, we set frequency ranges from 0.01 Hz to 100 Hz.

2.1.4 Electrode peeling test

Graphite (SG17) and silicon-graphite composite (SiG, SJ advanced materials) are used as active materials. They are coated on copper foil (18 um) and dried at 150 °C in vacuum conditions. The loading level of each electrode is ~10.0 mg cm^{-2}, composite density is 1.6 g cm^{-3} and double-sided tapes (3M300LSE, W: 25 mm) attached to the one side of slide glass and electrode surfaces. The electrodes are detached by constant speed (150 mm min^{-1}) horizontally by a tension test equipment (5943, INSTRON). This peeling tests was carried out by international organization for standardization (ISO) 29862.

2.2 Electrochemical analysis

The anode electrode was consisted of anode powder (95 wt.%), Super-P (1 wt.%), carboxymethyl cellulose (2 wt.%), and styrenebutadiene rubber (2 wt.%) with distilled water. In case of silicon nanopowders (Alfa Aesar), the electrodes were consisted of 80 wt.% SNPs , 10 wt.% Super-p, 5 wt.% carboxymethyl cellulose and 5 wt% styrenebutadiene rubber. These powders were mixed by using homogenizer. Active material powder and carbon black were premixed using mortar then mixed with CMC powders by using homogenizer (5,000 rpm, 45 min) after adding D.I. water. Lastly, SBR particles were dispersed to the suspension. The mixed suspension was coated on Cu-foil (18um) with doctor-blade then, the electrode was pressed to set electrode density (~ 1.6 g cm^{-3}) and dried in vacuum oven at 150°C for 6 hrs. The anode loading level was ~10.0 mg cm^{-2}. The positive electrode was prepared by mixing the cathode powder (96 wt.%), Super-P (2 wt.%), and poly(vinylidene fluoride) binders (2wt.%) in N-methyl-2-pyrrolidinon. The cathode loading level and electrode density were ~26.0 mg cm^{-2} and ~3.0 g cm^{-3}, respectively. This cathode electrode dried in vacuum oven at 120°C.

Used electrolyte was 1.15 M $LiPF_6$ with ethylene carbonate (EC), ethylmethyl carbonate (EMC) dimethylene carbonate (DMC) in 2: 4: 4 volume ratio which also includes diisopropylfluorophosphate (DFP) 1 wt.% and vinyl carbonate (VC) 1 wt.% as additives. Both coin half and full-cell were assembled in a dry argon atmosphere globe box. The electrochemical performances were tested using CR2032 coin half-cell, coin full-cell, and pouch type full-cell. The separator was polypropylene (PP)/ polyethylene (PE)/ PP composite (Celgard). In case of half-cell, the charge-discharge voltage ranges were from 0.005 V to 1.5 V vs. Li/Li^+. Before charge-discharge cycle tests, the cells were galvanostatically discharged to 0.005 V at 0.1 C rate and maintained at 0.005 V until the current decreased to 0.01 C rate, then charged to 1.5 V at 0.1 C rate. This step is called formation and were carried out twice. In case of full-cell, the charge-discharge voltage windows were from 4.2 V to 2.8 V vs. Li/Li^+. Before charge-discharge cycle tests, the cells were galvanostatically charged to 4.2 V at 0.1 C rate and maintained at 4.2 V until the current decreased to 0.01 C rate, then discharged to 2.8 V at 0.1 C rate. This formation step was carried out twice and the cycle performance at 25°C was evaluated charge and discharge C-rate of 1C.

2.3 Instrumental analysis

The electrochemical impedance spectroscopy (EIS) of CR2032 coin half-cell were measured from 0.01 Hz to 1 MHz frequency with 1mV sinus amplitude at 0.15 V, SOC 100%, and SOC 100% after formation. The viscosity of binder solutions was measured by viscometer (DV-Ⅱ+ Pro, BROOKFIELD) according to concentration. The electrode thickness was measured by in situ measurement of electrochemical dilatometry. The cell is pouch full-cell type which consists of SiG composite as anode materials and NCM 622 as cathode materials. The morphology of peeled electrodes were analyzed by scanning electron microscopy (SEM, verios 460, FEI). Cross-sectional images of the anode particles were obtained by using focused ion beam (FIB, NX2000, HITACHI). The structural and chemical analysis for SEI layers and composite structures of CMC/SBR was performed by using a high resolution transmission electron microscopy (HR-TEM, ARM300F, JEOL).

III. Results and discussions

3.1 The effects of high molecular weight CMC binder to physical properties of electrodes

Figure 14a and table 2 show size distribution of hydrodynamic radius with diameters 1,938 nm, 3,580 nm, and 5,560 nm for H-MW CMC, M-MW CMC, and L-MW CMC, respectively by using a DLS instrument. These samples were measured by diluting a concentration with 0.01 wt.% to prevent extrinsic inter-molecular interactions such as collisions, electrostatic interactions among particles. It was considered that H-MW CMC with long chain length has more extended size of hydrodynamic radius due to its rigid carbon backbones. Figure 14b shows zeta-potential with diluted solution with concentration 0.01wt.%. The exposed anionic carboxylate groups induce negative charges at the double layer interphases. H-MW CMC has extended chains which have less amount of exposed anionic groups in the solvent, leading more positive potentials than that of L-MW CMC. It was believed that L-MW CMC has high-gradient dispersion in aqueous solutions because of its anchored chains. Figure 14b and table 2 represent values of surface potentials of -81.2 mV, -60.8 mV, and -33.8 mV respectively. From figure 14a and 14b, it is proved that the chain lengths affect to size of dynamic hydration radius.

Large volumes of H-MW CMC induce inter-molecular interactions which were attributed by van der Waals forces. Figure 15 shows the viscosity of different molecular weight with following concentrations. The viscosity of different molecular weight CMC solutions were evaluated by using viscometer with variation of concentration. As shown in figure 15, H-MW CMC has the highest viscosity at the same concentration as well as increasing rate of concentration. It indicates that the inter-molecular interactions of H-MW CMC are more favorable than that of L-MW CMC.

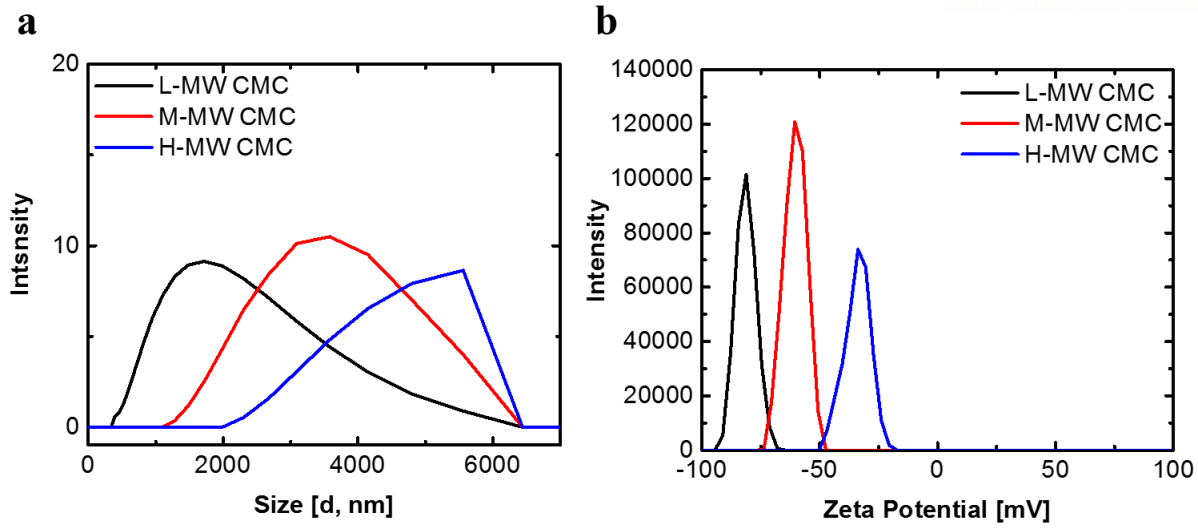

Figure 14. (a) Dynamic light scattering (DLS) data of L-MW CMC, M-MW CMC, and H-MW CMC at 25°C. (b) Zeta-potential data of three kinds of CMC solutions at 25°C.

	L-MW CMC	M-MW CMC	H-MW CMC
Z-average (nm)	1,938	3,580	5,560
Zeta-potential (mV)	-81.2	-60.8	-33.8

Table 2. The average values of Z-average and zeta-potential of each CMC solutions at 25°C.

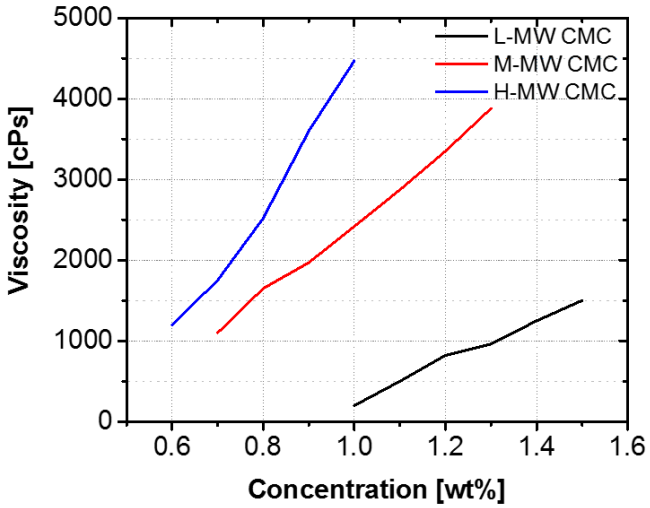

Figure 15. Viscosity vs. concentration curves of each CMC solutions at 25°C.

We analyzed the influences on chain length to rheological properties of each slurry by using viscometer. The rheological performances are evaluated to define stability of slurry, which could be attributed to the inter-molecular interactions. Viscoelasticity is dynamic mechanical analysis where a sinusoidal fluctuation is applied to microstructures. From frequency sweep modes, we set frequency ranges from 0.01Hz to 100Hz. Figure 16a and 16b are storage modules and loss modules curves respectively. Storage moduli (G') represents elastic features and loss moduli (G'') indicates viscous properties. The storage moduli value of slurry with H-MW CMC of 2.79 is higher than that with L-MW CMC of 2.06 at high shear rate. Also, the loss moduli with H-MW CMC is higher than L-MW CMC at high rate. Both storage and loss modules with H-MW CMC are more retained stably at high shear rate, while that of L-MW CMC lost its rheological properties even at low shear rate. In addition, H-MW CMC exhibits a cross-over point (yield point) at high shear rate. This is because long chain polymer molecules prevent disintegrations of polymer–particle network at high shear perturbations.

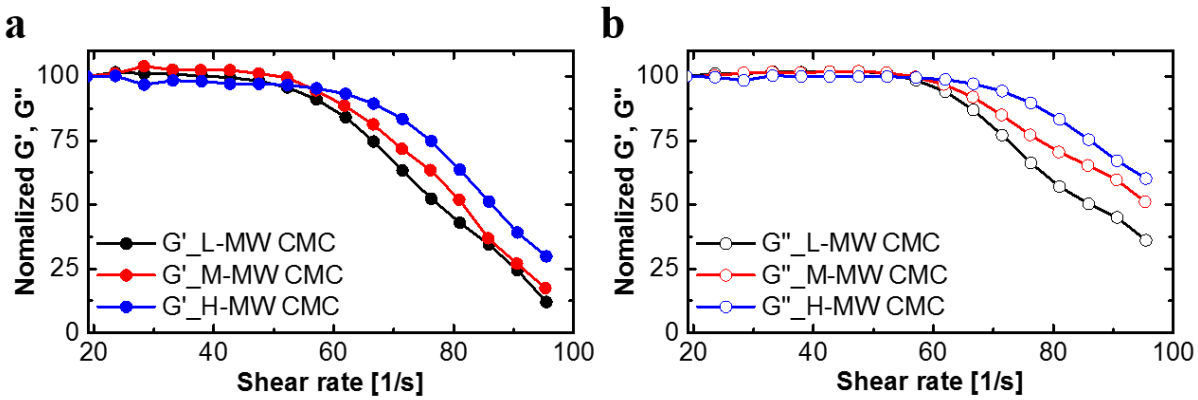

Figure 16. (a) Normalized storage moduli (Pa) vs. shear rate (s^{-1}) curves. (b) Normalized loss moduli (Pa) vs. shear rate (s^{-1}) curves.

Storage (G'), Loss (G'') Moduli (Pa)	L-MW CMC		M-MW CMC		H-MW CMC	
	G'	G''	G'	G''	G'	G''
Low rate	17.13	22.26	11.92	19.71	9.35	17.93
High rate	2.06	8.04	2.08	10.08	2.79	10.79
Decreases ratio (%)	87.97	63.88	82.55	48.86	70.16	39.82

Table 3. The values of storage (G'), loss (G'') moduli (Pa) and the decreasing ratio of each moduli from low shear rate to high shear rate.

In addition, surface zeta potential differences between active materials and binder influence on adsorption ability. The adsorption test was carried out using TOC instruments, which could measure concentration changes of supernatant in centrifuged suspensions. Figure 17a shows that the absorbed amount to the graphite with H-MW CMC is 2 times higher than that of L-MW CMC. It is because H-MW CMC has more positive zeta potential value of -33.8 mV than that of L-MW CMC, -81.2 mV so, H-MW CMC could be more adsorbed on the surface of graphite which has a highly negative surface potential. As seen from figure 17b, dispersed H-MW CMC in the solvents has less amount of exposed anionic functional groups per unit volume due to its extended structure. H-MW CMC leads stronger electrostatic interactions with graphite than L-MW CMC that could reduce electrolyte decomposition at the surface of active materials.

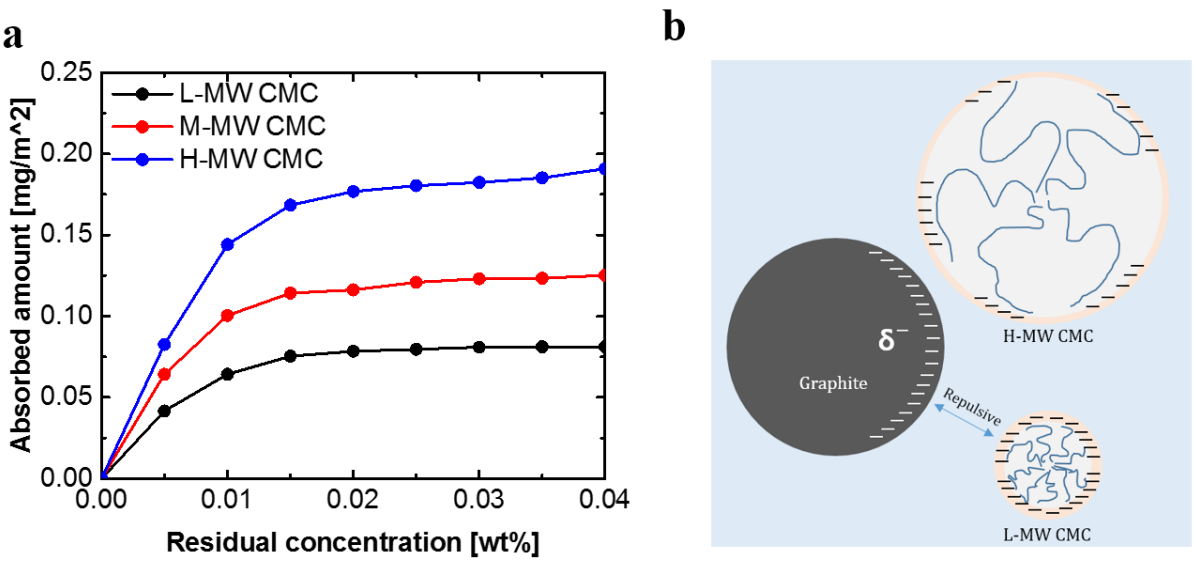

Figure 17. (a) Adsorption isotherm curves for graphite with different CMC binders. (b) Illustrations of adsorption mechanism for H-MW CMC and L-MW CMC.

Generally, polymeric binders, one of the major components in an electrode, were used to connect particles and modify the surface of active materials.[23] The binding force is attributed by nature of binders such as chain length, DS, and functional groups. The hydroxyl and carboxylate functional groups of extended polymer chains could contain many particles per one molecule, suggesting improved adhesion. The adhesion between active materials and counter collector is the main issue for high capacity active materials such as silicon and alloying type materials because of severe volume expansion resulting in pulverizations and breakdown of electrical networks. Commonly, the adhesion strength is highly dependent on the structures of binder composites and will be strong with the

increasing size of conformation. Figure 18a shows the adhesion strengths for electrodes measured by INSTRON equipment with peeling speed of 150 mm min^{-1}. Figure 18b shows processes of peeling test according ISO 29862 by a simple illustration. As shown in figure 18a, adhesion forces of an electrode with H-MW CMC is much higher than that of L-MW CMC (8.32 and 5.90 gf mm^{-1} respectively). Figure 18c, 18d, 18e are the SEM image of peeled electrodes on the copper foil side for L-MW CMC, M-MW CMC, and H-MW CMC respectively. The electrode with L-MW CMC has low adhesion ability between active materials and current collectors compared with H-MW CMC which has many adhered active materials onto the current collectors. It was believed that strong van der Waals forces of H-MW CMC improve high adhesion ability and strong intermolecular interaction. The strong physical properties such as adsorption and adhesion are desirable for high energy density anode materials because electrochemical performances such as cycle ability and rate capability of silicon materials are directly related to mechanical failure of electrode.

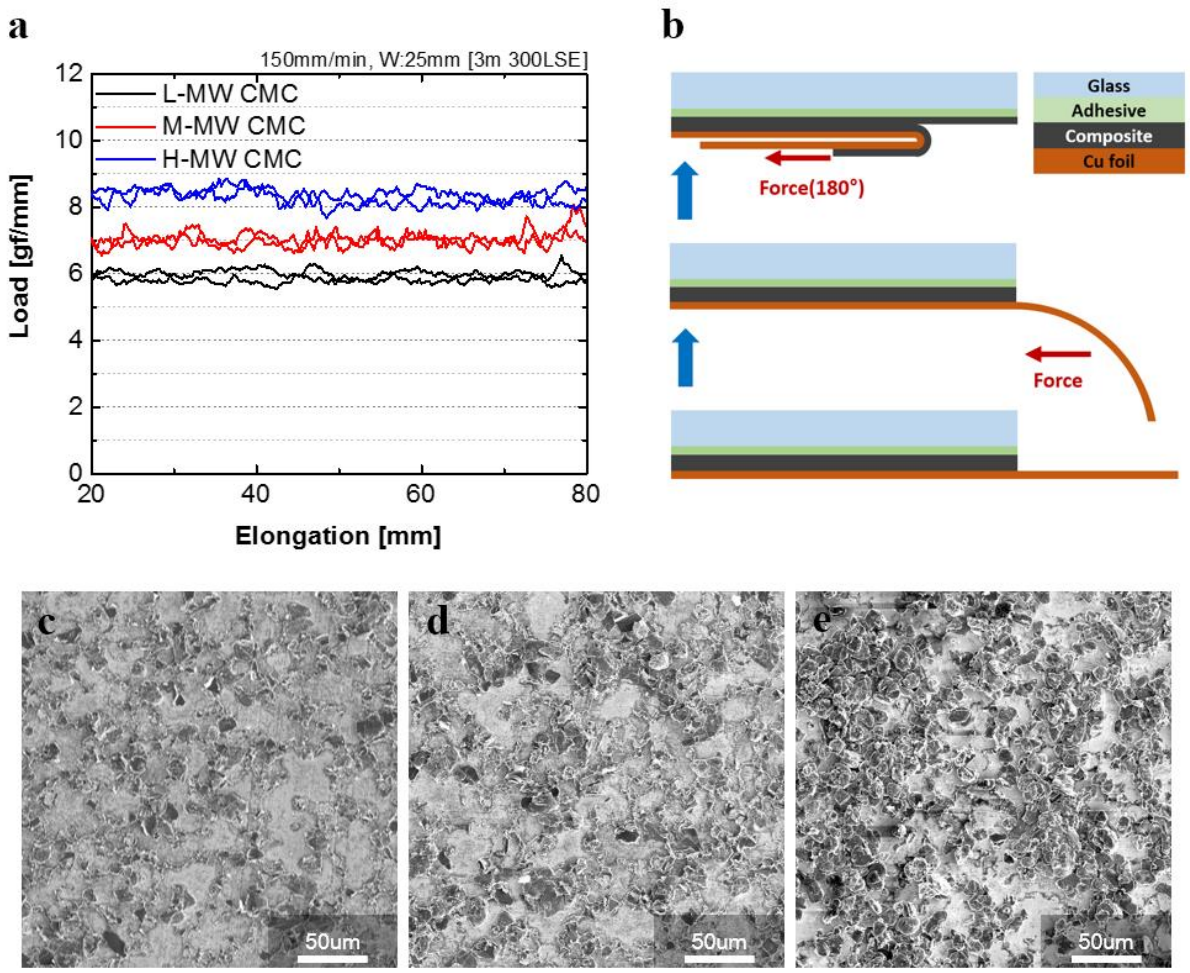

Figure 18. (a) The adhesion strengths for electrodes measured by INSTRON equipment with peeling speed of 150 mm min^{-1}. (b) Illustration of peeling test according ISO 29862. The SEM images of peeled electrodes on the copper foil side for (c) L-MW CMC (d) M-MW CMC (e) H-MW CMC.

3.2 The effects of high molecular weight CMC binder to electrochemical performances

The first cycle formation voltage profiles of H-MW CMC, M-MW CMC, and L-MW CMC are shown in figure 19a. The loading levels of electrodes are 1.62 mg cm^{-2} and current densities are 3.5mAh cm^{-2}. Figure 19a shows that charge capacity of SNPs anode with H-MW CMC (3,076 mAh g^{-1}) is higher than that of L-MW CMC (2,899 mAh g^{-1}). It also shows that the initial coulombic efficiency of SNPs electrode with H-MW CMC has higher value of 87.87% than L-MW CMC, 83.73%. It indicates that strong mechanical properties of H-MW CMC could prevent degradation of electrode integrity, resulting from volume changes upon cycling. This suggests that H-MW CMC is anticipated to play an important role which could form dense and compact SEI layers. Figure 20 shows electrochemical impedance spectroscopy (EIS) data for graphite, silicon-graphite composite (SiG), and silicon nanopowders (SNPs). These are tested at 0.15 V during first discharge, SOC 100%, and SOC 100% after formation. As shown in figure 20i, SEI resistance of the electrode with H-MW CMC (77.54 Ω) is smaller than that of L-MW CMC (95.90 Ω), indicating that high integrity of electrode sustains the composite structure during volume changing.

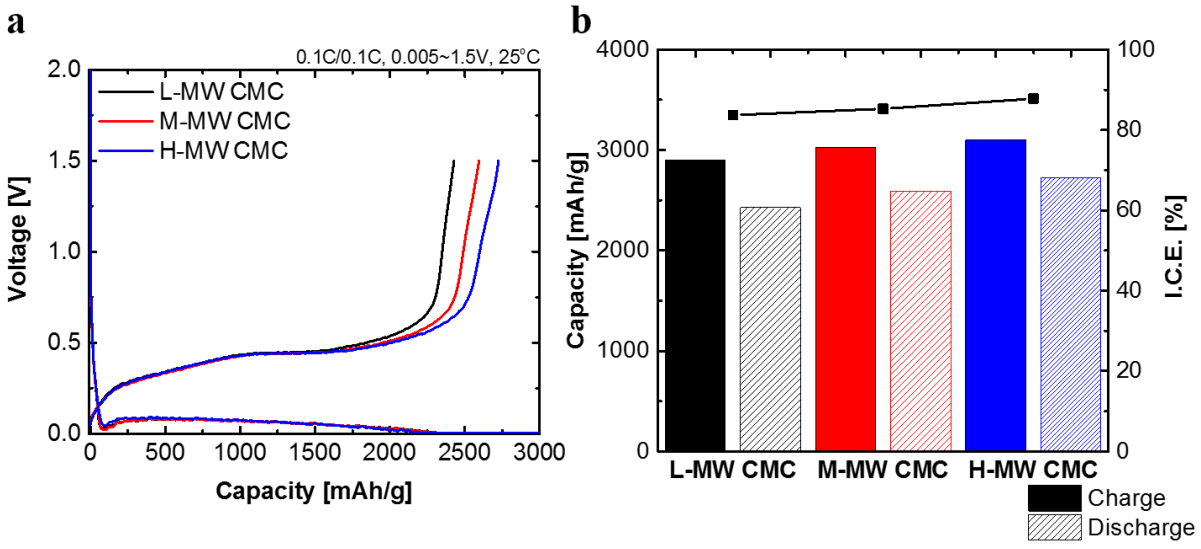

Figure 19. (a) Charge and discharge potential curves for silicon nanoparticles at first cycle from 1.5 V to 0.005 V in a coin-type half cell at 25°C. (b) The graphs of capacity and initial coulombic efficiency (I.C.E.) for each electrodes with different molecular weight CMC binders.

	Charge capacity (mAh g^{-1})	Discharge capacity (mAh g^{-1})	Initial coulombic efficiency (%)
L-MW CMC	2,899	2,428	83.73
M-MW CMC	3,050	2,614	85.70
H-MW CMC	3,076	2,703	87.87

Table 4. Values of charge and discharge capacity (mAh g^{-1}) and initial coulombic efficiency (%) for each SNP anode electrodes with different molecular weight CMC binders.

To further evaluate the effect of molecular weight on surface resistances, we used graphite, SiG composite, and SNPs as anode materials. As shown in figure 20j, SEI resistances of all three materials with H-MW CMC are larger than that of L-MW CMC before lithiation, at 0.15 V. This result shows that surface film resistance with H-MW CMC is larger than that of L-MW CMC due to more covered surface with polymeric binders which hinder lithium diffusion. However, figure 20k shows that the surface resistance of SiG composite and SNPs anodes with H-MW CMC is lower than that of L-MW CMC at fully charged state. In contrast, the resistance of graphite anode with H-MW CMC is still higher than that of L-MW CMC. From these results, the surface resistance is attributed by lithiation reactions, resulting in volume changes. It suggests that strong mechanical strength of H-MW CMC retains integrity of electrodes, which prevents continuous growth of SEI layers, resulting from particle pulverization and electrode fractures with silicon materials during first charging. The stable SEI layers are desirable for enhanced life time and durability upon cell operation.

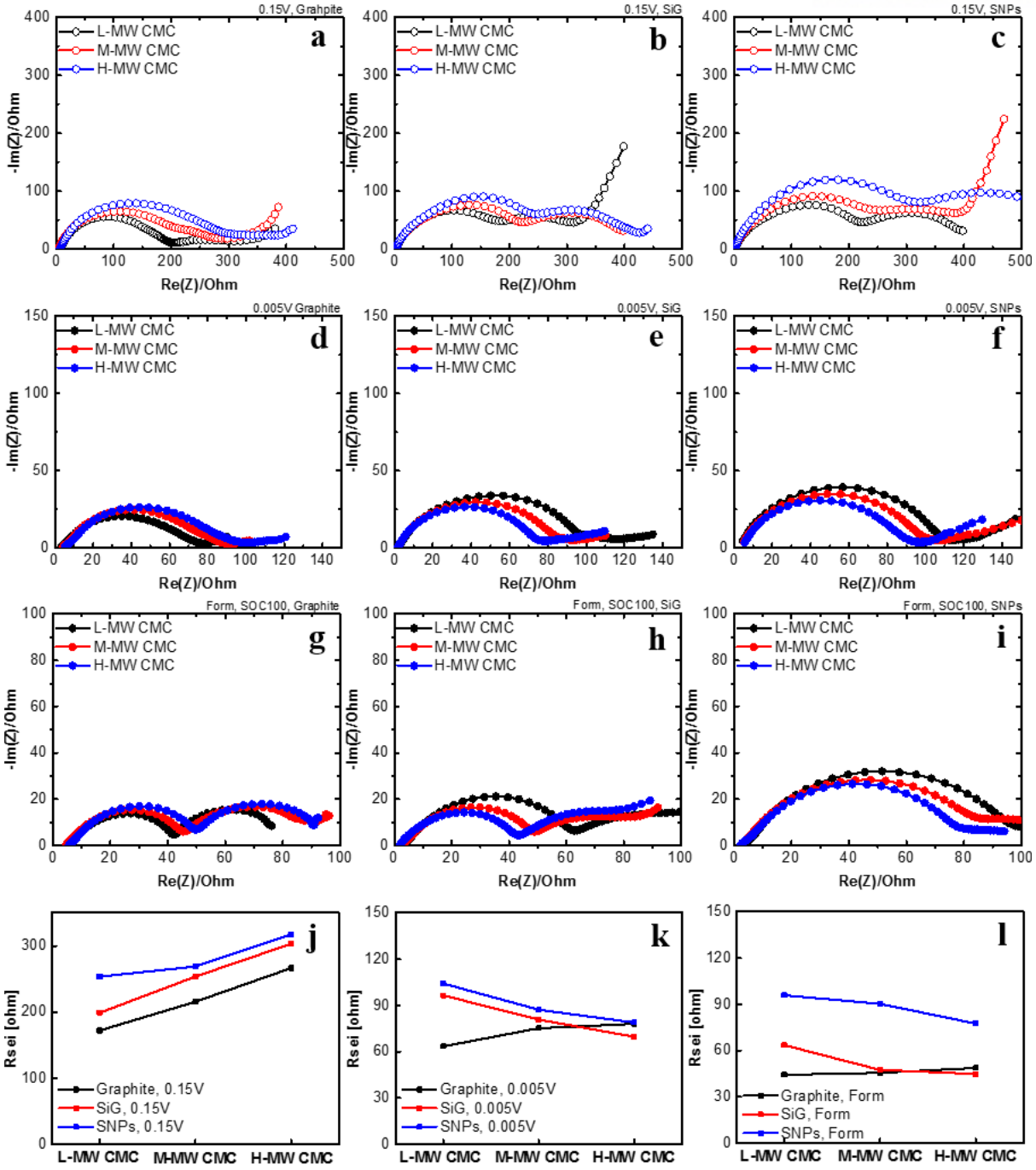

Figure 20. Electrochemical impedance spectroscopy (EIS) data for graphite, silicon-graphite composite (SiG) and silicon nanopowders (SNPs). These are tested at 1) before lithiation at 0.15 V, 2) SOC 100%, and 3) SOC 100% after formation. (a) Graphite at 0.15V, (b) SiG at 0.15V, (c) SNPs at 0.15V, (d) Graphite at SOC 100%, (e) SiG at SOC 100%, (f) SNPs at SOC 100%, (g) Graphite at SOC 100% after formation, (h) SiG at SOC 100% after formation, (i) SNPs at SOC 100% after formation. The film resistances at (j) 0.15 V, (k) 0.005 V, (l) 0.005V after formation for graphite, SiG, and SNPs.

		R_{SEI} (at 0.15V)	R_{SEI} (SOC100%)	R_{SEI} (SOC100% after formation)
Graphite	L-MW CMC	172.11	63.48	44.41
	M-MW CMC	215.73	75.31	45.69
	H-MW CMC	266.55	78.15	48.80
SiG	L-MW CMC	198.94	96.50	63.60
	M-MW CMC	253.61	80.86	47.53
	H-MW CMC	303.27	69.68	44.97
Silicon	L-MW CMC	253.61	104.21	95.90
	M-MW CMC	268.90	87.24	90.34
	H-MW CMC	317.45	78.96	77.54

Table 5. Values of surface film resistances (SEI layer resistances) calculated by Z-view programs. The unit is ohm, Ω.

As seen from figure 21a and 21b, anodes with L-MW CMC which were cycled shows thicker SEI layers than that of L-MW CMC. To further evaluate SEI layer, the cycled electrodes were examined by cross-sectional observation using HR-TEM after FIB etching process. Figure 21c, 21d displays HR-STEM images of two electrode samples, H-MW CMC and L-MW CMC. The SEI layer thickness of L-MW CMC is approximately 20nm and it has rough morphology. In contrast, a morphology of SEI layer with H-MW CMC is uniform and dense structures, results in low SEI resistances with thickness of 13nm. This result attributed to strong interaction between SiG composite and H-MW CMC, elevating mechanical integrity at the surface of SiG particles.

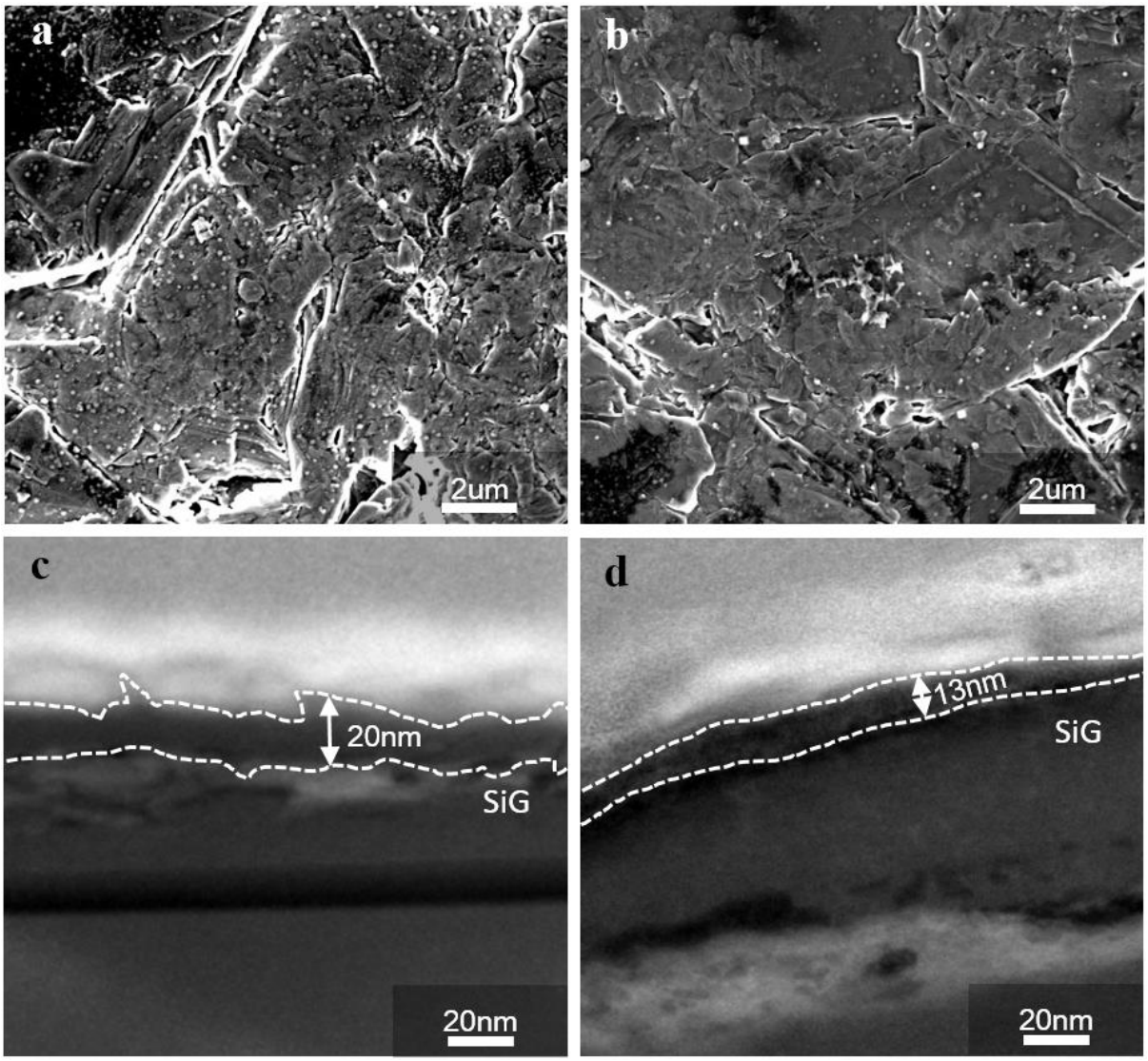

Figure 21. STEM images for electrodes with (a) H-MW CMC and (b) L-MW CMC which was milled by focused ion beam (FIB) after formation. The dotted lines represent solid electrolyte interphase (SEI) layers.

The thickness changes of pouch full-cell with SiG composite and NCM 622 were measured to verify the ability of binders for accommodating huge volume expansions upon cycling. Figure 22a is the illustration for *in situ* measurement of the electrode swelling with electrochemical dilatometry. The pouch-type full cell was galvanostatically charged and discharged where the voltage range is from to 4.2 V to 2.8V. The cells were charged at 0.1 C rate and maintained at 4.2 V until the current decreased to 0.02 C rate then, rested during 4 hrs then discharged to 2.8V at 0.1 C rate. At this step, the cell with H-MW CMC has volume expansion value of 0.107 % and that with L-MW CMC was 0.130%. The cells which charged at 0.2 C rate during 2 hrs and discharged at 0.2C rate. Then the cells were charged

at 0.2 C rate and 0.5C rate respectively and maintained at 4.2 V until the current decreased to 0.05 C rate and discharged at 0.2C rate. The cells were cycled from 4.2V to 2.8V at 0.5 C rate and has constant voltage (CV) modes which were maintained at 4.2 V until the current decreased to 0.05 C rate. Figure 22b shows the degree of the electrode swelling during formation, charge, and discharge cycles. As shown in figure 22a, the cell with H-MW CMC anodes has less volume changes during formation and cycling. It was due to strong mechanical forces of H-MW CMC which prevents electrode fractures and particle pulverization. With these favorable features of H-MW CMC, the cells with H-MW CMC show better cycle performances than that of L-MW CMC. Figure 23a is cycle curves for H-MW CMC and L-MW CMC respectively. The SiG anodes with H-MW CMC show cycle retention of 70.03% at 300 cycles, while L-MW CMC has low cycle retention of 66.42% at 300 cycles.

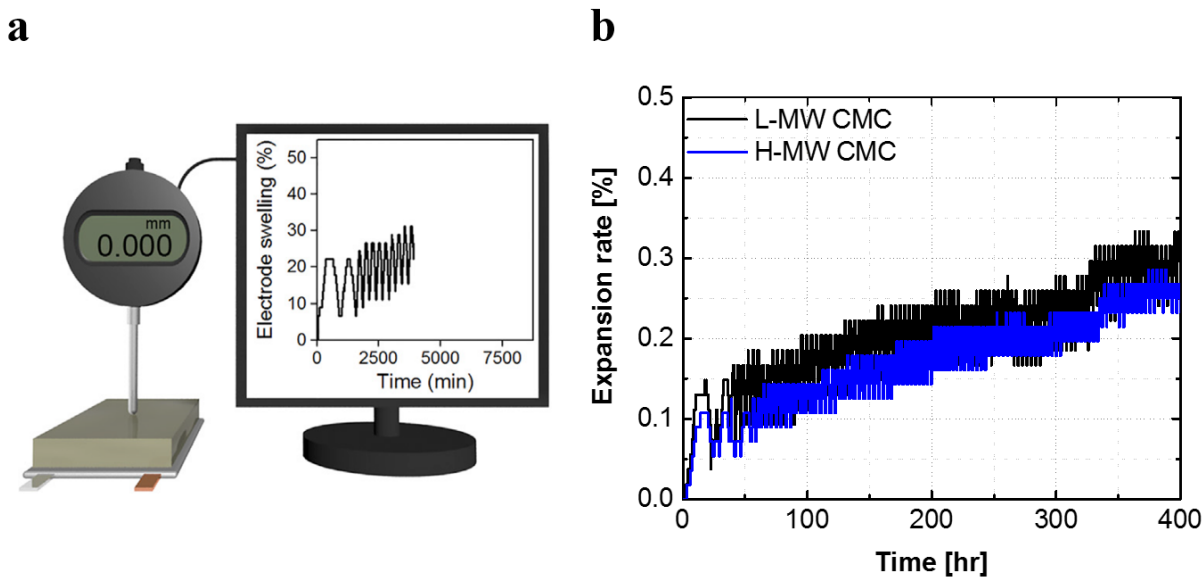

Figure 22. (a) *In situ* measurement of the electrode swelling with electrochemical dilatometry. (b) The thickness variation of pouch-type full cell during formation, charge, and discharge cycles.

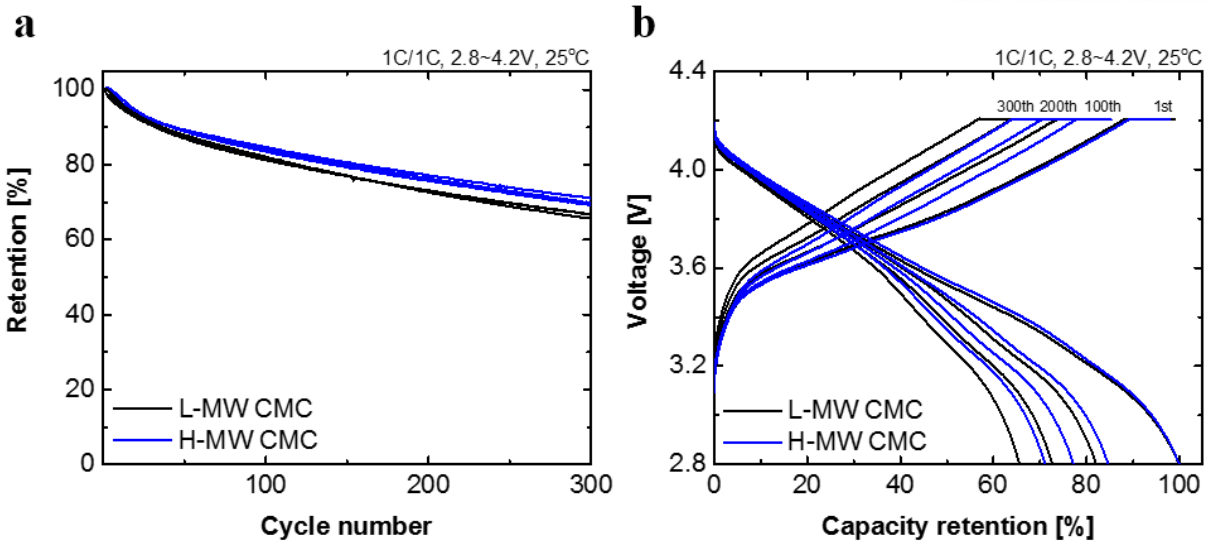

Figure 23. (a) Cycle curves for H-MW CMC and L-MW CMC. (b) Voltage profiles at each 1st, 100th, 200th, 300th cycles for H-MW-CMC and L-MW CMC.

To further evaluate the effect of H-MW CMC binder on active materials, we analyzed CMC/SBR thin films. These films consisted of CMC and SBR with 1:1 compositions and its thickness was approximately 30~150 nm. Figure 24a is the SEM image of SBR thin film and figure 24b is that of CMC/SBR composite film. Figure 24c and 24d are STEM images of L-MW CMC/SBR composite thin films and H-MW CMC/SBR composite thin films respectively. Figure 24a and 24b show that the SBR particles with diameter of 120 nm were aggregated by adding CMC binder. As shown in figure 24c, the composite structures with L-MW CMC has many pores and loosen morphology, indicating easily deformed structures which could not sustain mechanical integrity. In contrast, H-MW CMC/SBR composite shows compact and dense structures like honeycomb. It implies that H-MW CMC adsorbed to the surface of active materials with more dense and hard structure to modify surface of active materials. It proved that H-MW CMC could form stable and thin SEI layers and improve mechanical integrity of electrode and cycle ability.

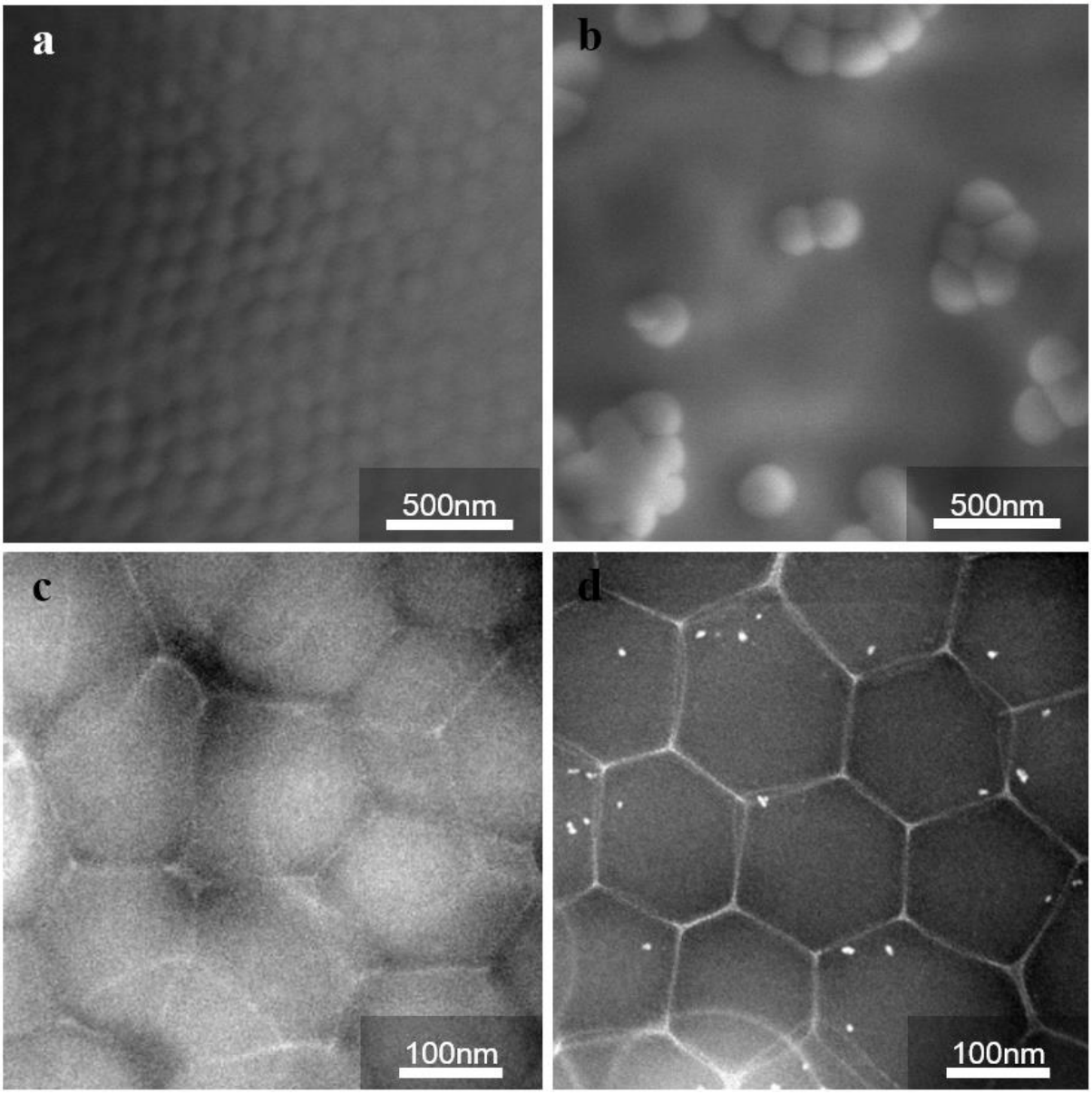

Figure 24. SEM images of (a) SBR thin film and (b) CMC/SBR composite film. STEM images of (c) L-MW CMC/SBR composite thin films and (d) H-MW CMC/SBR composite thin films.

3.3 The interaction between SBR and CMC binder.

Herein, the effects of a binder ratio between CMC and SBR for electrode fabrications were analyzed by SEM, HR-TEM, EDX, and EELS. Figure 25 shows that SEM images for each peeled pristine electrode by an INSTRON equipment with compositions of 96:3:1, 96:2:2, and 96:1:3 respectively. The secondary electron microscopic mode and back scattering electron microscopic mode were represented owing to compare degrees of adhesion for each electrodes. As shown in figure 25, the adhesion between particles and current collector was increased due to SBR binders which sank to the bottom of the electrodes during dry process. In contrast, the adhesion among particles in the electrode composite was improved due to CMC binder which forms interaction forces among particles such as active materials, conducting agents, and binders. These particles were embedded to large conformation of CMC binder, resulting in rigid composite structures.

To further figure out the effects of CMC/SBR compositions on mechanical strength, energy dispersive X-ray spectroscopy (EDX) and electron energy loss spectroscopy (EELS) results were attained using HR-TEM. Figure 26 shows EDX mapping results of CMC/SBR composite thin films, showing aggregation structures. As shown in figure 26, SBR particles were embedded in CMC binder films, indicating that the CMC binder network retains SBR particles in binder composites.

As shown in figure 27a, there is no special chemical interaction between CMC and SBR, indicating only physical aggregation. The low intensity was observed in CMC films due to its thin thickness, while SBR particle has a diameter of 120nm, leading a high intensity. As seen from figure 26, CMC binder observed at the interphases between SBR particles, leading physical aggregation.

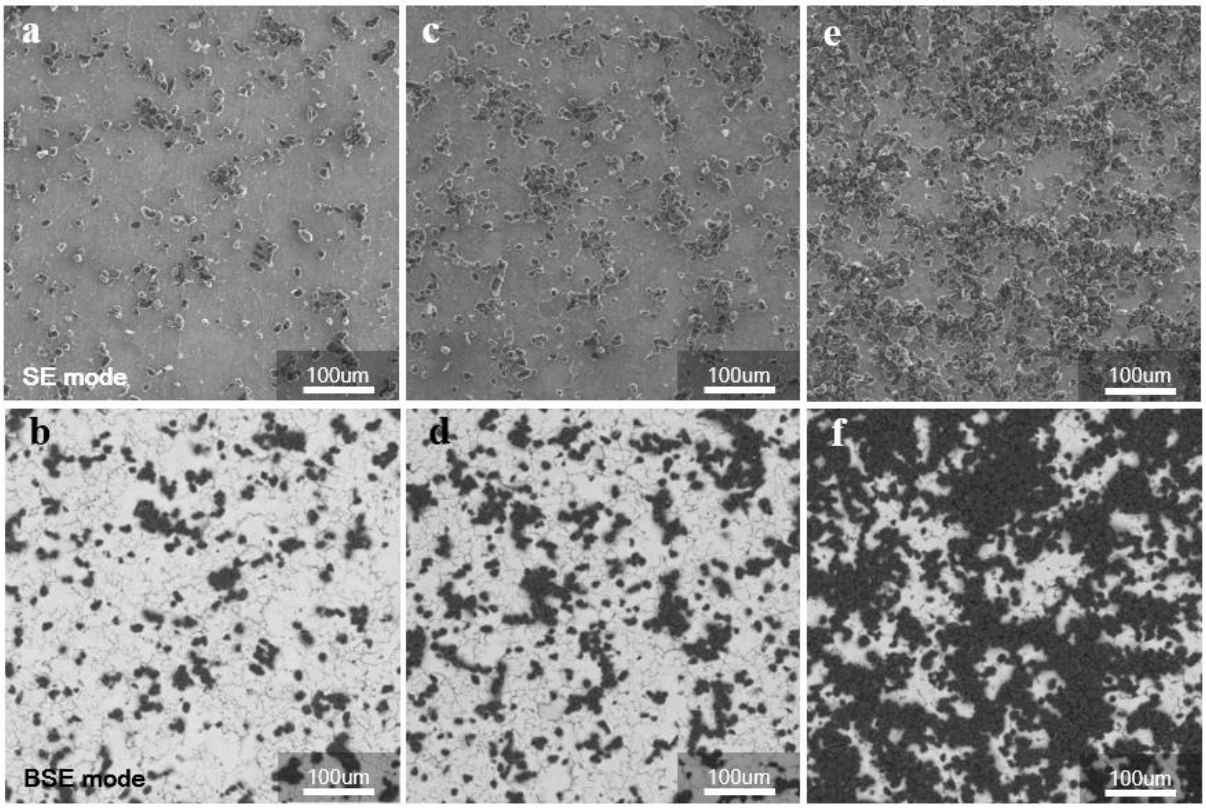

Figure 25. SEM images of copper foil side of graphite pristine electrode peeled by INSTRON equipment. (a), (b) 96:3:1 (Graphite:CMC:SBR, wt.%) compositions, (c), (d) 96:2:2, (e), (f) 96:1:3.

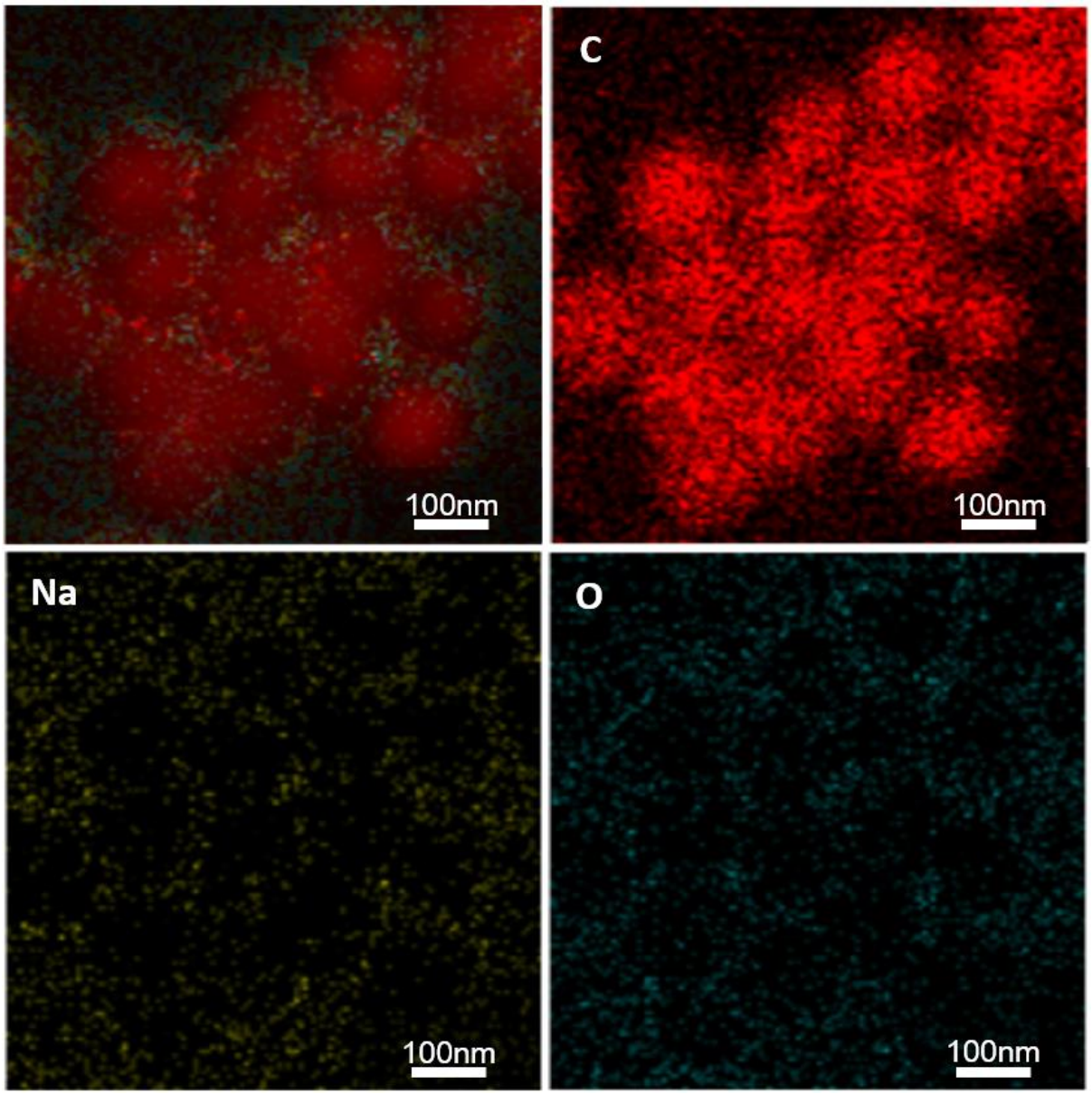

Figure 26. EDX images of H-MW CMC/SBR composite thin films.

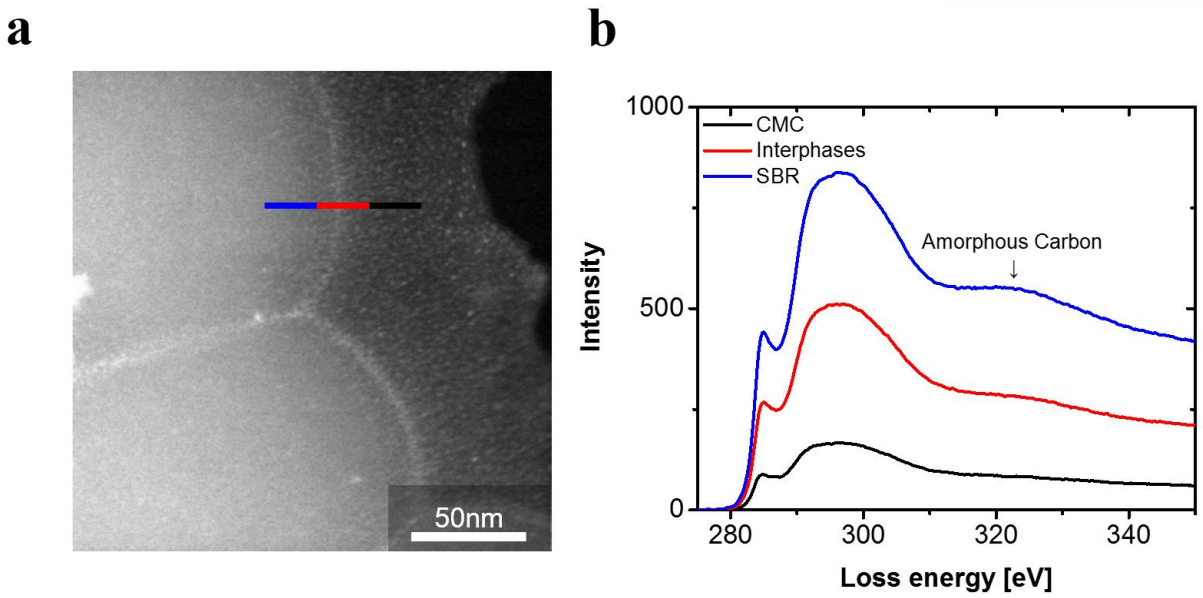

Figure 27. (a) The image of high-resolution STEM for H-MW CMC/SBR composite thin films. (b) Electron energy loss spectroscopy (EELS) graphs for CMC, SBR, and the interface between CMC and SBR.

IV. Conclusions

In summary, the better mechanical integrity of electrode and electrochemical performances of H-MW CMC seem to result from large size of conformation, high stiffness binder networks, and strong intermolecular interaction. The size of conformation of dispersed H-MW CMC was 5,560 nm and that with L-MW CMC was 1,938 nm. Large conformation enhances inter-molecular interaction between dispersed polymers in the solvents, resulting from high van der Waals forces. In addition, more positive surface zeta-potential of H-MW CMC, -33.8 mV, induce the driving forces for adsorption with surface of active materials which have highly negative surface energy. The adhesion forces of H-MW CMC were enhanced, leading strong interaction with active materials and current collectors. It showed better electrochemical performances such as cycle retention, stable SEI, and high coulombic efficiency. From the *In situ* measurement of the electrode swelling with electrochemical dilatometry, it was proved that H-MW CMC enhances the integrity of silicon-graphite anodes. Recently, with ever-growing interest in electric vehicles and energy storage systems, high capacity anode materials have been treated as promising materials. From the perspective of high energy density, H-MW CMC can mitigate particle pulverization and electrode failure of silicon-based materials, leading improved mechanical integrity of electrodes.

V. References

1. Larcher, D.; Tarascon, J. M., Towards greener and more sustainable batteries for electrical energy storage. *Nature Chemistry* **2014,** *7*, 19.

2. Roy, P.; Srivastava, S. K., Nanostructured anode materials for lithium ion batteries. *Journal of Materials Chemistry A* **2015,** *3* (6), 2454-2484.

3. Dunn, B.; Kamath, H.; Tarascon, J.-M., Electrical Energy Storage for the Grid: A Battery of Choices. **2011,** *334* (6058), 928-935.

4. Winter, M.; Besenhard, J. O.; Spahr, M. E.; Novák, P., Insertion Electrode Materials for Rechargeable Lithium Batteries. **1998,** *10* (10), 725-763.

5. Nitta, N.; Yushin, G., High-Capacity Anode Materials for Lithium-Ion Batteries: Choice of Elements and Structures for Active Particles. *Particle & Particle Systems Characterization* **2014,** *31* (3), 317-336.

6. Park, M.-H.; Kim, M. G.; Joo, J.; Kim, K.; Kim, J.; Ahn, S.; Cui, Y.; Cho, J., Silicon Nanotube Battery Anodes. *Nano Letters* **2009,** *9* (11), 3844-3847.

7. Wu, H.; Cui, Y., Designing nanostructured Si anodes for high energy lithium ion batteries. *Nano Today* **2012,** *7* (5), 414-429.

8. Sun, Y.; Liu, N.; Cui, Y., Promises and challenges of nanomaterials for lithium-based rechargeable batteries. **2016,** *1*, 16071.

9. Chae, S.; Ko, M.; Kim, K.; Ahn, K.; Cho, J., Confronting Issues of the Practical Implementation of Si Anode in High-Energy Lithium-Ion Batteries. *Joule* **2017,** *1* (1), 47-60.

10. Obrovac, M. N.; Chevrier, V. L., Alloy Negative Electrodes for Li-Ion Batteries. *Chemical Reviews* **2014,** *114* (23), 11444-11502.

11. Kim, H.; Seo, M.; Park, M.-H.; Cho, J., A Critical Size of Silicon Nano-Anodes for Lithium Rechargeable Batteries. **2010,** *49* (12), 2146-2149.

12. Liu, N.; Lu, Z.; Zhao, J.; McDowell, M. T.; Lee, H.-W.; Zhao, W.; Cui, Y., A pomegranate-inspired nanoscale design for large-volume-change lithium battery anodes. *Nature Nanotechnology* **2014,** *9*, 187.

13. Tadros, T., Interaction forces between particles containing grafted or adsorbed polymer layers. *Advances in Colloid and Interface Science* **2003,** *104* (1), 191-226.

14. Munao, D.; van Erven, J. W. M.; Valvo, M.; Garcia-Tamayo, E.; Kelder, E. M., Role of the binder on the failure mechanism of Si nano-composite electrodes for Li-ion batteries. *Journal of Power Sources* **2011,** *196* (16), 6695-6702.

15. Park, H.-K.; Kong, B.-S.; Oh, E.-S., Effect of high adhesive polyvinyl alcohol binder on the anodes of lithium ion batteries. *Electrochemistry Communications* **2011,** *13* (10), 1051-1053.

16. Koo, B.; Kim, H.; Cho, Y.; Lee, K. T.; Choi, N.-S.; Cho, J., A Highly Cross-Linked

Polymeric Binder for High-Performance Silicon Negative Electrodes in Lithium Ion Batteries. *Angewandte Chemie International Edition* **2012,** *51* (35), 8762-8767.

17. Wang, C.; Wu, H.; Chen, Z.; McDowell, M. T.; Cui, Y.; Bao, Z., Self-healing chemistry enables the stable operation of silicon microparticle anodes for high-energy lithium-ion batteries. *Nature Chemistry* **2013,** *5*, 1042.

18. Wu, M.; Xiao, X.; Vukmirovic, N.; Xun, S.; Das, P. K.; Song, X.; Olalde-Velasco, P.; Wang, D.; Weber, A. Z.; Wang, L.-W.; Battaglia, V. S.; Yang, W.; Liu, G., Toward an Ideal Polymer Binder Design for High-Capacity Battery Anodes. *Journal of the American Chemical Society* **2013,** *135* (32), 12048-12056.

19. Song, J.; Zhou, M.; Yi, R.; Xu, T.; Gordin, M. L.; Tang, D.; Yu, Z.; Regula, M.; Wang, D., Interpenetrated Gel Polymer Binder for High-Performance Silicon Anodes in Lithium-ion Batteries. **2014,** *24* (37), 5904-5910.

20. Jeschull, F.; Brandell, D.; Wohlfahrt-Mehrens, M.; Memm, M., Water-Soluble Binders for Lithium-Ion Battery Graphite Electrodes: Slurry Rheology, Coating Adhesion, and Electrochemical Performance. *Energy Technology* **2017,** *5* (11), 2108-2118.

21. Hochgatterer, N. S.; Schweiger, M. R.; Koller, S.; Raimann, P. R.; Wöhrle, T.; Wurm, C.; Winter, M., Silicon/Graphite Composite Electrodes for High-Capacity Anodes: Influence of Binder Chemistry on Cycling Stability. *Electrochemical and Solid-State Letters* **2008,** *11* (5), A76-A80.

22. Huang, S.; Ren, J.; Liu, R.; Yue, M.; Huang, Y.; Yuan, G., The progress of novel binder as a non-ignorable part to improve the performance of Si-based anodes for Li-ion batteries. **2018,** *42* (3), 919-935.

23. Drofenik, J.; Gaberscek, M.; Dominko, R.; Poulsen, F. W.; Mogensen, M.; Pejovnik, S.; Jamnik, J., Cellulose as a binding material in graphitic anodes for Li ion batteries: a performance and degradation study. *Electrochimica Acta* **2003,** *48* (7), 883-889.

24. Lee, J.-H.; Paik, U.; Hackley, V. A.; Choi, Y.-M., Effect of Carboxymethyl Cellulose on Aqueous Processing of Natural Graphite Negative Electrodes and their Electrochemical Performance for Lithium Batteries. *Journal of The Electrochemical Society* **2005,** *152* (9), A1763-A1769.

25. Liu, W.-R.; Yang, M.-H.; Wu, H.-C.; Chiao, S. M.; Wu, N.-L., Enhanced Cycle Life of Si Anode for Li-Ion Batteries by Using Modified Elastomeric Binder. *Electrochemical and Solid-State Letters* **2005,** *8* (2), A100-A103.

26. Wang, J.; Somasundaran, P., Adsorption and conformation of carboxymethyl cellulose at solid–liquid interfaces using spectroscopic, AFM and allied techniques. *Journal of Colloid and Interface Science* **2005,** *291* (1), 75-83.

27. Buqa, H.; Holzapfel, M.; Krumeich, F.; Veit, C.; Novák, P., Study of styrene butadiene rubber and sodium methyl cellulose as binder for negative electrodes in lithium-ion batteries. *Journal*

of Power Sources **2006,** *161* (1), 617-622.

28. Chen, L.; Xie, X.; Xie, J.; Wang, K.; Yang, J. J. J. o. A. E., Binder effect on cycling performance of silicon/carbon composite anodes for lithium ion batteries. **2006,** *36* (10), 1099-1104.

29. Lestriez, B.; Bahri, S.; Sandu, I.; Roué, L.; Guyomard, D., On the binding mechanism of CMC in Si negative electrodes for Li-ion batteries. *Electrochemistry Communications* **2007,** *9* (12), 2801-2806.

30. Li, J.; Lewis, R. B.; Dahn, J. R., Sodium Carboxymethyl Cellulose: A Potential Binder for Si Negative Electrodes for Li-Ion Batteries. *Electrochemical and Solid-State Letters* **2007,** *10* (2), A17-A20.

31. Komaba, S.; Yabuuchi, N.; Ozeki, T.; Han, Z.-J.; Shimomura, K.; Yui, H.; Katayama, Y.; Miura, T., Comparative Study of Sodium Polyacrylate and Poly(vinylidene fluoride) as Binders for High Capacity Si–Graphite Composite Negative Electrodes in Li-Ion Batteries. *The Journal of Physical Chemistry C* **2012,** *116* (1), 1380-1389.

32. Kierzek, K. J. J. o. M. E.; Performance, Influence of Binder Adhesion Ability on the Performance of Silicon/Carbon Composite as Li-Ion Battery Anode. **2016,** *25* (6), 2326-2330.

33. Bridel, J. S.; Azaïs, T.; Morcrette, M.; Tarascon, J. M.; Larcher, D., Key Parameters Governing the Reversibility of Si/Carbon/CMC Electrodes for Li-Ion Batteries. *Chemistry of Materials* **2010,** *22* (3), 1229-1241.

34. Khraisheh, M.; Holland, C.; Creany, C.; Harris, P.; Parolis, L., Effect of molecular weight and concentration on the adsorption of CMC onto talc at different ionic strengths. *International Journal of Mineral Processing* **2005,** *75* (3–4), 197-206.

35. Mazouzi, D.; Lestriez, B.; Roué, L.; Guyomard, D., Silicon Composite Electrode with High Capacity and Long Cycle Life. **2009,** *12* (11), A215-A218.

36. Vogl, U. S.; Das, P. K.; Weber, A. Z.; Winter, M.; Kostecki, R.; Lux, S. F., Mechanism of Interactions between CMC Binder and Si Single Crystal Facets. *Langmuir* **2014,** *30* (34), 10299-10307.

37. Zhang, S. S.; Xu, K.; Jow, T. R., EIS study on the formation of solid electrolyte interface in Li-ion battery. *Electrochimica Acta* **2006,** *51* (8), 1636-1640.

38. Komaba, S.; Ozeki, T.; Okushi, K., Functional interface of polymer modified graphite anode. *Journal of Power Sources* **2009,** *189* (1), 197-203.

39. Verma, P.; Maire, P.; Novák, P., A review of the features and analyses of the solid electrolyte interphase in Li-ion batteries. *Electrochimica Acta* **2010,** *55* (22), 6332-6341.

40. Nirmale, T. C.; Kale, B. B.; Varma, A. J., A review on cellulose and lignin based binders and electrodes: Small steps towards a sustainable lithium ion battery. *International Journal of Biological Macromolecules* **2017,** *103* (Supplement C), 1032-1043.

41. Zhang, S.; Ding, M. S.; Xu, K.; Allen, J.; Jow, T. R., Understanding Solid Electrolyte Interface Film Formation on Graphite Electrodes. *Electrochemical and Solid-State Letters* **2001,** *4* (12), A206-A208.

42. Menkin, S.; Golodnitsky, D.; Peled, E., Artificial solid-electrolyte interphase (SEI) for improved cycleability and safety of lithium–ion cells for EV applications. *Electrochemistry Communications* **2009,** *11* (9), 1789-1791.

43. An, S. J.; Li, J.; Daniel, C.; Mohanty, D.; Nagpure, S.; Wood, D. L., The state of understanding of the lithium-ion-battery graphite solid electrolyte interphase (SEI) and its relationship to formation cycling. *Carbon* **2016,** *105*, 52-76.